

STANNIC: Systolic STochAstic ONliNe SchedulIng AcCelerator

ADAM H. ROSS, Electrical and Computer Eng. Dept, University of Illinois Chicago, USA

VAIRAVAN PALANIAPPAN, Electrical and Computer Eng. Dept, University of Illinois Chicago, USA

DEBJIT PAL, Electrical and Computer Eng. Dept, University of Illinois Chicago, USA

Efficient workload scheduling is a critical challenge in modern heterogeneous computing environments, particularly in high-performance computing (HPC) systems. Traditional software-based schedulers struggle to efficiently balance workloads due to *scheduling overhead*, *lack of adaptability to stochastic workloads*, and *suboptimal resource utilization*. The scheduling problem further compounds in the context of shared HPC clusters, where *job arrivals* and *processing times* are inherently stochastic. Prediction of these elements is possible, but it introduces additional overhead. To perform this complex scheduling, we developed two FPGA-assisted hardware accelerator microarchitectures, HERCULES and STANNIC. HERCULES adopts a task-centric abstraction of stochastic scheduling, whereas STANNIC inherits a schedule-centric abstraction. These hardware-assisted solutions leverage *parallelism*, *pre-calculation*, and *spatial memory* access to significantly accelerate scheduling. We accelerate a non-preemptive stochastic online scheduling algorithm to produce heterogeneity-aware schedules in near real time.

With HERCULES, we achieved a speedup of *up to 1060×* over a baseline C/C++ implementation, demonstrating the efficacy of a hardware-assisted acceleration for heterogeneity-aware stochastic scheduling. With Stannic, we further improved efficiency, achieving a *7.5×* reduction in latency per computation iteration and a *14×* increase in the target heterogeneous system size. Experimental results show that the resulting schedules demonstrate efficient machine utilization and low average job latency in stochastic contexts.

CCS Concepts: • **Do Not Use This Code** → **Generate the Correct Terms for Your Paper**; *Generate the Correct Terms for Your Paper*; Generate the Correct Terms for Your Paper; Generate the Correct Terms for Your Paper.

Additional Key Words and Phrases: Hardware Accelerator, Stochastic Online Scheduling, High-Performance Computing, Systolic Architecture

ACM Reference Format:

Adam H. Ross, Vairavan Palaniappan, and Debjit Pal. 2018. STANNIC: Systolic STochAstic ONliNe SchedulIng AcCelerator. *J. ACM* 37, 4, Article 111 (August 2018), 30 pages. <https://doi.org/XXXXXXXX.XXXXXXX>

1 Introduction

In modern high-performance computing environments, heterogeneous processing elements (PEs) such as Central Processing Units (CPUs), Graphics Processing Units (GPUs), Field-Programmable Gate Arrays (FPGAs), Neural Processing Units (NPU), and other application-specific accelerators are increasingly being deployed to meet the demands of diverse computing tasks. These systems promise improved performance and energy efficiency by scheduling tasks to the most suitable

Authors' Contact Information: Adam H. Ross, aross50@uic.edu, Electrical and Computer Eng. Dept, University of Illinois Chicago, Chicago, Illinois, USA; Vairavan Palaniappan, vpala8@uic.edu, Electrical and Computer Eng. Dept, University of Illinois Chicago, Chicago, Illinois, USA; Debjit Pal, dpal2@uic.edu, Electrical and Computer Eng. Dept, University of Illinois Chicago, Chicago, Illinois, USA.

Permission to make digital or hard copies of all or part of this work for personal or classroom use is granted without fee provided that copies are not made or distributed for profit or commercial advantage and that copies bear this notice and the full citation on the first page. Copyrights for components of this work owned by others than the author(s) must be honored. Abstracting with credit is permitted. To copy otherwise, or republish, to post on servers or to redistribute to lists, requires prior specific permission and/or a fee. Request permissions from permissions@acm.org.

© 2018 Copyright held by the owner/author(s). Publication rights licensed to ACM.

ACM 1557-735X/2018/8-ART111

<https://doi.org/XXXXXXXX.XXXXXXX>

PEs based on computation patterns and objectives. *However, scheduling in such heterogeneous PEs remains a fundamental and computationally complex challenge* [10, 23].

Unlike homogeneous systems, where scheduling primarily involves load balancing and fair resource allocation, heterogeneous systems introduce a complex multi-dimensional decision space – scheduling decisions must account for varying processing capabilities, task-PE affinities, execution time variability and unpredictability of tasks’ arrival, contention for shared PE resources, and in many cases, strict timing or energy constraints. Consequently, scheduling targeting heterogeneous systems becomes a complex *search and optimization* in multi-dimensional decision space as shown in Figure 1. Moreover, task characteristics are often not known in advance or may change at runtime, making *static or offline scheduling approaches impractical*. As the system complexity increases, the cost of making optimal or near-optimal scheduling decisions increases rapidly. ***These challenges demand fast, adaptive, scalable, scheduling technique capable of reasoning under uncertainty, all the while maintaining low computational overhead.*** Addressing these goals simultaneously is non-trivial and remains a critical bottleneck in leveraging the full potential of heterogeneous computing systems.

Recent scheduling techniques for heterogeneous systems aim to improve efficiency and load balancing, but they suffer from high scheduling overhead and inconsistent convergence [9, 11, 32]. Other schedulers offer adaptability but rely on predictive models and often neglect energy or scalability concerns [18]. More recent scheduling strategies [19, 21, 26, 34] provide strong theoretical guarantees but face limitations in dynamic environments, task diversity, and hardware applicability due to their overwhelming computational complexity. Overall, most existing methods are either too complex for real-time use, lack scalability, or fail to adapt under uncertainty.

In our previous work [22], we developed a *hardware-accelerated scheduler targeting heterogeneous computing resources to address the problem of efficient, low-overhead online scheduling in heterogeneous systems under unpredictable task arrival and runtime variability*. We leverage a simple and adaptable algorithm (Stochastic Online Scheduling Algorithm or SOSA) to address online scheduling in heterogeneous systems [13] and extend it to make it amenable for hardware implementation. We adopt a *task-centric* abstraction of SOSA in our prior work. A critical aspect of this algorithm is that it does not require precise task profiling; instead, it relies on estimates of processing time, making it practical for dynamic environments where such precise task information is often unavailable and/or unreliable but can be estimated with high confidence based on prior task history. Using this method in HERCULES, we were able to demonstrate efficient scheduling, while achieving up to 1093× speedup over software implementations of the same scheduling methodology.

In this work, we identify and address the shortcomings of our prior work and develop STANNIC to further optimize scheduling iteration speed, hardware resource utilization, and scalability through routing simplification. Crucially, we use the same SOSA algorithm [13] as the foundation for both hardware accelerator architectures, however, we adopt a *schedule-centric* abstraction to implement STANNIC. The architectural difference of STANNIC as compared to our prior work is primarily due to the different abstractions/perspectives of the SOSA algorithmic flow.

Specifically, we note the timing and routing overheads severely restricted the performance of the the pipeline architecture used in [22], and use this insight as motivation to devise a new

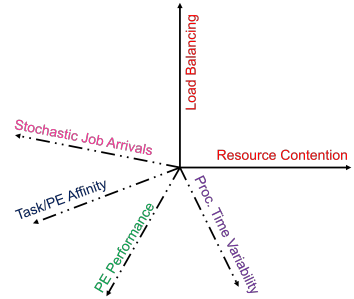


Fig. 1. **Illustration of the decision space for Stochastic, Online Heterogeneous Scheduling.** Load Balancing and Resource Contention are standard considerations in multi-machine scheduling, with the other axis presenting new considerations in heterogeneous system context.

systolic architecture for STANNIC that leverages the spatial locality of priority-ordered jobs. STANNIC outperforms our prior work with an average of $7.5\times$ less cycles per scheduling iteration, all while requiring fewer hardware components and routing, allowing STANNIC to scale to much larger system configurations than its predecessor, being capable of tracking up to 140 machines compared to HERCULES's maximum of 10.

In this paper, we make the following additional technical contributions over [22] to advance the field of stochastic online heterogeneous scheduling.

- (1) We systematically analyze our prior μ architecture, HERCULES, to localize various performance bottlenecks, and augment them to develop a new μ -architecture, STANNIC, to further optimize online stochastic scheduling performance.
- (2) We present an alternative, schedule-centric abstraction of the SOSA algorithmic flow to streamline memory access to significantly enhance computation performance.
- (3) We present an extensive set of experimental results demonstrating the effectiveness, efficiency, and adaptability of the SOSA in scheduling tasks with diverse characteristics on a set of heterogeneous computing resources in near real-time with a power envelope of 21 Watts, achieving over $1968\times$ speedup over a C/C++ baseline software implementation.
- (4) We present a set of quantitative comparison metrics for our two architectures, demonstrating performance improvements across design iterations.

The paper is organized as follows. Section 2 details preliminaries and necessary background knowledge and Section 3 discusses the scheduling algorithm and its discretization. Section 4 explains the HERCULES microarchitecture. (μ architecture) Section 5 analyzes HERCULES μ architecture and localizes various performance bottlenecks. Section 6 then presents the STANNIC μ architecture addressing the identified bottlenecks. Sections 7 and 8 discuss the experimental setup and results, respectively, which were performed to quantitatively compare and contrast the performance of the schedulers. Section 9 surveys the related work followed by our conclusion in Section 10.

2 Preliminaries and Background

In this section, first we present key conventions and definitions along with a representative example that we use throughout our work. Later in this section, we provide a high-level overview of the stochastic online scheduling algorithm [13]. Finally, we present necessary background on systolic architecture in our context.

Conventions: A computer program can be viewed as a sequence of instructions. In our formalization, we leave the definition of computer program implicit, but we will treat it as a pair $\langle I, t \rangle$ where $t \in \mathbb{Z}^+$. Informally, I represents the set of instructions and t represents the number of cycles required to execute I . Given a program $P = \langle I, t \rangle$, we will refer to t as execution time of P , denoted by $Time(P)$. A program P is *compute-bound* if majority of instructions are arithmetic/control instructions, *memory-bound* if majority of instructions are data movement, load/store, and memory operations, and *mixed*, if it has a balanced or near-balanced mix of compute-bound and memory-bound instructions.

Definition 1. A *Machine* M is an abstraction of a compute unit represented as a tuple $M = \langle \mathbf{T}, \mathbf{Q} \rangle$, where \mathbf{T} is the machine type and \mathbf{Q} is the machine quality and $\mathbf{T} \in [\text{CPU}, \text{GPU}, \text{Mixed}]$, $\mathbf{Q} \in [\text{Best}, \text{Worst}]$. Intuitively, for a given program P , if the execution times are $Time(P)_{\text{Best}}$ and $Time(P)_{\text{Worst}}$ with $Q = \text{Best}$ and $Q = \text{Worst}$, respectively, then $Time(P)_{\text{Best}} \ll Time(P)_{\text{Worst}}$.

Definition 2. A *Job* J is an abstraction of a program P with uncertain execution time represented as a quadruple $J = \langle W, \hat{\epsilon}, \mathcal{P}, ID \rangle$, where W is the weight of J , $\hat{\epsilon}$ is a list of expected processing times (EPT) (i.e., how long it would take for P to run on machine M) with $|\hat{\epsilon}| = N$ where N is the number of machines,

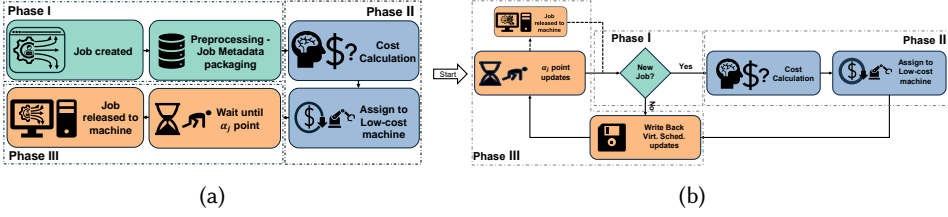


Fig. 2. **Stochastic Online Scheduling (SOS) Algorithmic Flows.** Figure 2a shows algorithmic flow for *stochastic online scheduling from a task centric perspective*. **Phase I** prepares a job for the scheduler, **Phase II** and **Phase III** show the steps involved in scheduling the job. Figure 2b revises the algorithmic flow involving the same functional steps but from a persistent, virtual-schedule perspective. Due to this re-framing, the algorithmic flow is now cyclical instead of linear as in Figure 2a. For clarity, the we used same phase labeling to demonstrate the functional similarity of the two algorithmic flows.

\mathcal{P} is the nature/bounding of a corresponding program P , i.e., $\mathcal{P} \in [\text{Compute}, \text{Memory}, \text{Mixed}]$, and $ID \in \mathbb{Z}^+$ is a unique job identifier. We use $J.W, J.\hat{\epsilon}$ to denote the individual components of a job J . We compute **weighted shortest processing time (WSPT)** of a job J for k^{th} machine as $T_k^J = J.W / \hat{\epsilon}_k$, $\hat{\epsilon}_k \in \hat{\epsilon} [13]$, which can be used to rank jobs by priority.

Intuitive Example: Lets consider a job J that corresponds to a convolution neural network layer being scheduled to a system that consists of just two machines, a CPU and a GPU. $J.\hat{\epsilon}$ would have two entries, one each corresponding to the expected processing time of J on either the CPU or GPU. Due to J being a convolutional operation, we could reasonably accomplish this job on either the CPU or the GPU, but we may expect the GPU implementation to complete quicker (i.e., $J.\hat{\epsilon}_{GPU} < J.\hat{\epsilon}_{CPU}$).

This EPT is a best guess, **not a guarantee**. For any actual job invocation, variance (i.e., from data loading, shared memory usage, etc.) will cause the actual runtime to deviate from this EPT. The Weight ($J.W$) of the job is an abstraction of this particular job's priority. We could encode it to account for metadata that may be known about this job. For example, Weight could correlate with the number of jobs that depend on the completion of this job, prioritizing the minimization of start delays. Alternatively, weight could correspond to a job's source, to establish priority for OS/Super User processes. Either way, Weight here is a global Prioritization metric, whereas EPT is a per-machine estimate of processing time.

Definition 3. A **Virtual Schedule (VS)** V_i for machine M_i is a partial order for the execution of a set of jobs $\{K\}$, reflecting the relative WSPT value (and thus priority) of the jobs in $\{K\}$. This is called a Virtual Schedule, because it contains all of the jobs that have been **assigned to a machine**, but have **not yet been released to the work queue**. It is an interim schedule where the ordering of jobs within it is still malleable. We use $Head.V_i$ to denote the head of V_i .

Intuitive Example: Let's reconsider the job discussed in the example of Definition 2. We established that in our example case that $J.\hat{\epsilon}_{GPU} < J.\hat{\epsilon}_{CPU}$, and so we shall assume that we assigned it to the GPU. However, while we are waiting to commit the job to the GPU for execution, another job K is introduced to the system. K is also assigned to the GPU, and while $K.\hat{\epsilon}_{GPU} = J.\hat{\epsilon}_{GPU}$, $K.W > J.W$. As such, the new job has a higher overall priority than job J . The Virtual Schedule allows us to adjust our planned schedule to reflect this, as the jobs have not yet been committed to a work queue.

2.1 Overview of Stochastic Online Scheduling (SOS) Algorithm

The **key intuition** behind the Greedy Stochastic Online Scheduling Algorithm (SOS) [13] is to compute the cost (in terms of expected delay) of assigning an incoming job to a machine M based on the *currently available resources*, *prior assigned jobs*, and *job priorities*, before greedily and irrevocably assigning the job to the machine with the lowest cost for execution. This is performed in three primary phases, which we describe in Section 2.1.1, and then reframe to the Virtual Schedule centric perspective in Section 2.1.2.

2.1.1 Stochastic Scheduling Algorithmic Flow from the Task-Centric Perspective. The SOS [13] focuses on on-the-fly intra- and inter-machine job scheduling. Figure 2a shows an overview of the SOS. The key objective of the SOS is to *minimize the weighted sum of the expected completion time* over a set of jobs in a greedy way. We discuss three phases of the SOS algorithm below.

Phase I (Preprocessing jobs): Sources produce new jobs either in burst mode or sequentially, however, the SOS algorithm considers a sequential job arrival during processing. The assumption of sequential job arrival allows the scheduler to tackle the uncertainty and/or stochasticity of jobs' arrival. The preprocessing steps append additional info to an arriving job, e.g., EPTs for a job ($J.\hat{\epsilon}$) for a set of target machines leveraging prior execution data or metadata obtained from the producers. Once a job is fully processed, it is released to the scheduler.

Phase II (Machine Assignment): The SOS computes the cost of assigning job J to machine M_i based on the expected delay of starting J and any other jobs already assigned to M_i (i.e., the jobs currently in V_i). The cost calculation consists of two components – $cost^H$ (delay on the new job from the set of earlier jobs (σ^H) with higher or equal priority in the V_i , (c.f., Section 3.1 for more details) and $cost^L$ (delay on set of earlier jobs (σ^L) with lower priority in the V_i). Both costs are cumulative across their respective sets (σ^H and σ^L) of assigned jobs. Internal priority is the relative WSPT value of J with respect to (w.r.t.) the other jobs assigned to M_i , which may appear in the Virtual Schedule V_i ahead of, behind, or in-between the other jobs. We explain J 's relative position in V_i w.r.t. other jobs in Section 3.1. Once the cost for each of the N machines has been calculated, the machine with the lowest cost is greedily and irrevocably chosen as the *assigned* machine for J .

Phase III (Job Scheduling): SOS also schedules all jobs assigned to a specific machine. Due to the stochastic and online nature of SOS, it is unknown when or if new jobs will be assigned. However, to ensure that future jobs that are shorter or more important can take precedent over previously assigned jobs, Jäger introduced the α_J WSPT policy, which tracks jobs in a Virtual Schedule V_i and adjusts ordering as new jobs come in [13]. The V_i then releases the job at its head ($Head.V_i$) when the wait time of $Head.V_i \geq (\alpha_J \times J.\epsilon_i)$, $\alpha_J \in (0, 1]$. Once J has been released from the Virtual Schedule, it is released to the end of the assigned machine's actual job queue, and is considered fully scheduled for execution.

Shortcomings of the Task-Centric Perspective of the SOS Algorithm: Although presenting the algorithmic flow from the task-centric perspective is useful in understanding the overarching flow of the greedy SOS, it does not inherently translate well into a dedicated hardware scheduling architecture; Though functionally, jobs arriving and then leaving scheduled to a machine is the primary goal of a scheduler, *this model does not consider the data flow of the persistent internal states* which inform the majority of the schedulers cost decisions. While we did this for our previous work in HERCULES [22], it leads to poor memory usage and routing congestion leading to a degraded overall performance (c.f., Section 5).

2.1.2 Re-Framing Stochastic Scheduling Algorithmic Flow from the Virtual Schedules Perspective. For our new model, which is shown in Figure 2b, we instead consider the virtual schedules perspective as the scheduling operation is performed. This re-framing shifts the focus away from the transient

elements of the algorithm (namely the scheduled jobs) and instead shifts it onto the persistent elements, the intermediary virtual schedules, enabling much more efficient utilization of memory elements and reducing routing congestion due to enhanced spatial/temporal locality. In this re-framed version, we still maintain the notions of the three phases of scheduling. However, instead of the flow being a pipeline where jobs come in and the assignment of that job is returned, this new flow projects the algorithm as a cyclical one, in which possible sources of alterations (*e.g.*, a new job J being assigned to machine M) to the virtual schedule are stepped through and considered, before finally being written back to establish the state of the virtual schedules for the next cycle.

In adapting this perspective for the algorithmic flow, we place a higher emphasis on the tracking and coherency of the persistent values that are necessary for every cycle of operation, including cycles in which a new job does not arrive. Using this model as the foundation for a new μ architecture design, we optimize the memory management of associated computations, thereby greatly reducing the spatial and temporal management overheads and enhancing scheduler performance.

2.2 Systolic Architectures

Systolic Architecture is a parallel computational architecture realized with multiple, identical, and simple PEs that rhythmically process and pass data mimicking the regularity of blood flow in heart [24]. These PEs are interconnected with their immediate neighbors, and as such are particularly useful for the acceleration of tasks with high spatial data interdependence. Each PE can perform local processes, and then “pump” their data along to other PEs as necessary for the completion of a given task (*c.f.*, Figure 3). To prototype the Virtual Schedule perspective of the SOS algorithm, we infuse systolic architecture in STANNIC.

Systolic architectures have been successfully used in several, diverse acceleration applications. Google’s Tensor Processing Units (TPUs) utilize a systolic architecture for acceleration of matrix multiplication in neural networks [28]. Another neural network example is Eyeriss [4], which specifically focuses on energy efficiency by maximizing spatial memory reuse during convolution. Yu et al., used a systolic architecture for DNA pattern matching [35], while [8, 25] both use a systolic architecture for efficient pattern recognition and vision transformers aiming for real-time execution [8] and power efficiency [25]. Additionally, recent design automation tools such as SuSy [17] and Allo [3] provide foundational support to generate optimized systolic designs. In each of these works, a spatial data dependency is leveraged to achieve acceleration.

As discussed in Section 2.1.2, the SOS maintains ordered V_i ’s over time in successive iterations while the scheduler is active, and in **Phase II** of the algorithm, the relative ordering of incoming job J effects the cost contributions of all other jobs K in V_i . As such, for STANNIC, we propose a systolic architecture that exploits this spatial relationship to optimize scheduling time.

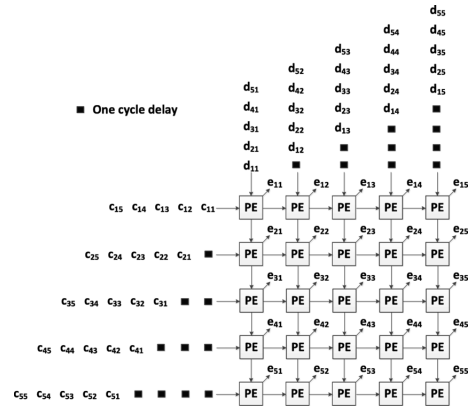


Fig. 3. **Systolic Flow Example.** A 5×5 systolic array for matrix multiplication [33]. Each PE is responsible for accumulating the value of its corresponding index in the output matrix e . To do this, each PE cascades row data from input matrix c to their right neighbor and column data from input matrix d to their downward neighbor.

3 Computational Mathematics of SOS in Continuous and Discrete Time

In this section, we first elaborate the cost computation for machine assignment for continuous time (Section 3.1). Next, we explain the enhancements and approximations to extend the cost computation to discrete time, making it amenable for hardware implementation (Section 3.2).

$$\iota_K(t_J) = 1 - \frac{1}{K \cdot \hat{\epsilon}_i} \cdot \overbrace{\int_0^{t_J} F_K^{V_i}(s) ds}^{\Omega}, \quad K \in V_i \quad (1)$$

$$F_K^{V_i}(s) = \begin{cases} 1, & \text{if } J \in \text{Head}.V_i \text{ at time } s \\ 0, & \text{otherwise} \end{cases}$$

3.1 Cost Computation in Continuous Time

The notion of **Virtual Work** (VW) is crucial for computing the cost of scheduling a job in a machine. Intuitively, VW captures the amount of time a job K has spent at the head of the Virtual Schedule ($\text{Head}.V_i$). The Ω in Equation (1) captures the amount of Virtual Work of job K completed at time t_J (i.e., when job J is created) and $\iota_K(t_J)$ represents the remaining fraction of Virtual Work of K . The VW is directly related to the α_J release point of that assigned job, as α_J sets the percentage threshold of completed Virtual Work at which the job is released (i.e., Phase III in Figure 2a).

The cost of scheduling job J in machine M_i , $\text{cost}(J \rightarrow M_i)$, denoted as cost for brevity, is computed as follows [13].

$$\text{cost} = (J.W) \cdot \left(J \cdot \hat{\epsilon}_i + \overbrace{\sum_{K \in V_i, T_i^K \geq T_i^J} \iota_K(t_J) \cdot K \cdot \hat{\epsilon}_i}^{\text{cost}^H} \right) + \overbrace{\sum_{K \in V_i, T_i^K < T_i^J} K.W \cdot \iota_K(t_J) \cdot J \cdot \hat{\epsilon}_i}^{\text{cost}^L} \quad (2)$$

The cost in Equation (2) has two parts – cost^H and cost^L . cost^H captures the set of jobs (σ^H) in V_i whose WSPT ratio is higher than or equal to the WSPT of J and cost^L captures the set of jobs (σ^L) in V_i whose WSPT ratio is lower than or equal to the WSPT of J . σ^H would delay the start of the job J as they have the higher WSPT priority whereas σ^L will be delayed by J as they have lower WSPT priority. This splitup of jobs in two sets is crucial to the performance of the cost calculation and non-trivial as the two sets of jobs affect the cost computation differently. Note that both cost^H and cost^L include the term $\iota_K(t_J)$. Intuitively, w.r.t. cost calculation, $\iota_K(t_J)$ correlates to the percentage of job K 's wait time is left before being released from V_i , by tracking how much of $K \cdot \hat{\epsilon}_i$ it has waited. Inclusion of $\iota_K(t_J)$ reduces delay incurred by the previously assigned job K onto the new job J (or vice versa), by this ratio. This is due to K being closer to release from V_i , and thus incurring a reduced delay.

3.2 Cost Computation in Discrete Time

A key necessity to port the SOS algorithms to digital hardware (e.g., FPGA) is to discretize certain parameters such as time. This modification leads to a considerable reduction in the cost computation complexity resulting in a simpler yet high-efficiency hardware design with reduced logic footprint.

Quantizing time allows to rewrite the integration (Ω) in Equation (1) as $n_K(t_J) = \sum_0^{t_J} F_K^{V_i}(t_J)$, where $n_K(t_J)$ represents the number of cycles a job K has performed Virtual Work in V_i . We track and update $n_K(t_J)$ in every clock cycle due to its importance in cost calculation and α_J release point determination. Such update forgoes detailed job tracking (e.g., when a job was added in the

V_i), lengthy summations to compute $n_K(t_j)$, and complex reconstruction of V_i every time a new job is added to it in favor of a singular lookup. Substituting $n_K(t_j)$ for the integration in Equation (1), the remaining fraction of virtual work simplifies as follows.

$$\hat{i}_K(t_j) = 1 - \frac{n_K(t_j)}{K \cdot \hat{\epsilon}_i}, K \in V_i \quad (3)$$

Substituting $\hat{i}_K(t_j)$ in Equation (2), $cost^H$ and $cost^L$ simplify as follow.

$$cost^H = (J.W) \cdot (J \cdot \hat{\epsilon}_i + \underbrace{\sum_{K \in V_i, T_i^K \geq T_i^J} \overbrace{(K \cdot \hat{\epsilon}_i - n_K(t_j))}^{sum^H}}_{sum^{HI}}) \quad (4)$$

$$cost^L = J \cdot \hat{\epsilon}_i \cdot \underbrace{\sum_{K \in V_i, T_i^K < T_i^J} \overbrace{\left(K.W - n_K(t_j) \frac{K.W}{K \cdot \hat{\epsilon}_i} \right)}^{sum^L}}_{sum^{LO}} \quad (5)$$

Remark: Although we are subtracting terms in sum^H and sum^L , we do not risk of having a previously assigned job K contributing a negative cost to a potential job's calculation. For either sum^H or sum^L to reduce to 0, $n_K(t_j)$ would have to equal $K \cdot \hat{\epsilon}_i$. However, with the α_j release policy, K will be released from V_i either at or before this point, as the job releases when $n_K(t_j) \geq \alpha_j \cdot K \cdot \hat{\epsilon}_i$, and $\alpha_j \in (0, 1]$.

3.3 Additional Design-Based Optimizations

We optimize Equations (3), (4) and (5) further to optimize the computation for efficient hardware implementation.

- (1) **Reductions in Division Operations:** We store $T_i^K = K.W/K \cdot \hat{\epsilon}_i$ to reuse it to compute $cost^L$ and when comparing T_i^J to T_i^K to sort K in $cost^H$ and $cost^L$ for cost calculation. Additionally, the earliest possible time to calculate T_i^K is when job K is first created and $cost(K \rightarrow M_i)$ is calculated. When J is assigned to V_i , we store T_i^J until J is released from V_i . When combined, these optimizations save numerous computationally costly division operations.
- (2) **Incremental Update for Virtual Work:** In addition to $n_K(t_j)$, the sum^H and sum^L solely rely on the attributes of the job $K \in V_i$. Note $n_K(t_j)$ is essentially a cycle count since K has started its Virtual Work, requiring frequent updates. A key observation is that all other attributes of K (e.g., $\hat{\epsilon}_i$) are constants when $n_K(t_j)$ is updated. Consequently, we *initialize* sum^H to its maximum value of $K \cdot \hat{\epsilon}_i$ and *decrement* it by **1** in every cycle K is virtually worked on. For sum^L , we initialize it to its maximum value of $K.W$ and decrement it by T_i^K (note $T_i^K = K.W/K \cdot \hat{\epsilon}_i$ is the WSPT of K in machine M_i). These set of optimizations save considerable amount of lengthy summations and divisions contained in sum^H and sum^L of Equations (4) and (5) making it faster and amenable for hardware implementation. It is worth noting that updating of sum^H and sum^L happens in parallel with the α_j release checks, *overlapping* the processing time of these updates, and preventing the need for explicit evaluation across each job K when $cost(J \rightarrow M_i)$ is computed.

Remark. These are the optimizations utilized in both HERCULES anmd STANNIC μ architectures. STANNIC further leverages the systolic organization and spatial ordering of jobs K within each V_i

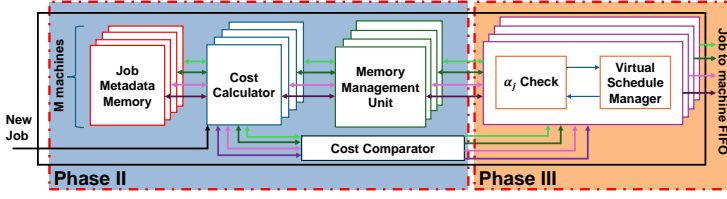


Fig. 4. **Top-level block diagram of the HERCULES scheduler.** Phase II and III are the phases shown in Figure 2a.

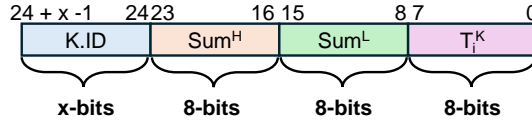


Fig. 5. **Job Metadata Memory register implementation.** x : Configurable based on the maximum number of jobs across all machines computed as $\lceil \log_2(M \times N) \rceil$. M : Number of machines. N : Max. number of jobs in V_i of machine M_i . This leads to a total register width of $x + 24$ bits.

to precalculate sum^{HI} (c.f., Equation (4)) and sum^{LO} (c.f., Equation (5)) for all possible separations of the high and low WSPT sets. The exact systolic mechanics that enable and maintain these pre-calculations will be discussed in Section 6.

4 HERCULES: Task-centric Hardware Implementation of SOS Algorithm

In this section, we discuss in detail the μ architectural components of HERCULES, the task-centric perspective (c.f., Section 2.1.1) hardware implementation of SOS algorithm.

4.1 HERCULES μ architecture

Figure 4 shows the μ architectural design of the scheduler in HERCULES. The scheduler implements Phase II and III of Figure 2a to identify the machine with the lowest compute cost and release the job to the machine at the designated α_j point. To compute the *cost* and track job progress in machine M_i , the following attributes for all jobs in the virtual schedule V_i needs to be retained – (i) $J.W$, (ii) $J.\hat{\epsilon}_i$ (iii) WSPT ratio (T_i^J), and (iv) α_j point until each job is released for execution. After a job is released, it no longer contributes to the cost calculation, and its metadata can be safely discarded by the scheduler. The Virtual Schedule must be updated in two events – (1) when a job is released for execution and (2) when a new job is scheduled. To perform these updates, the scheduler must track the job at the head of the Virtual Schedule ($Head.V_i$). **Job Metadata Memory** stores the job metadata and sum^H and sum^L ; the **Cost Calculator** interacts with Job Metadata Memory and computes $cost(J \rightarrow M_i)$; the **Cost Comparator** identifies the minimum-cost machine for job J ; the **Memory Management Unit** acts as a gatekeeper to this metadata to ensure consistent and efficient read/write access; the α_j **Check** module determines whether a job has reached its α_j scheduling threshold and is eligible for execution; and the **Virtual Schedule Manager** maintains the ordering of the jobs in the Virtual Schedule. In the next few subsections, we detail each μ architectural block.

4.1.1 Job Metadata Memory (JMM). The JMM is implemented as an $M \times N$ register array, where M is the number of machines and N is the maximum number of jobs that can reside in the V_i . A key insight is that each job's metadata must be accessed in every cycle for cost updates and scheduling decisions. A RAM-based implementation would impose limitations on simultaneous read and write

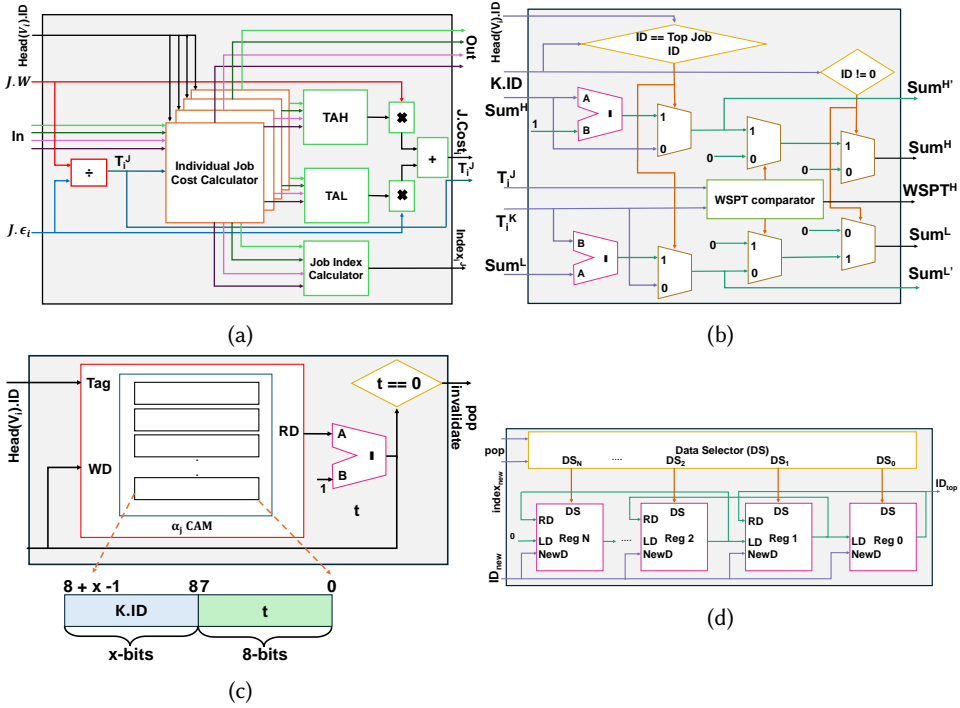


Fig. 6. μ architectural components of HERCULES. (a): **Cost Calculator**. TAH: Tree Adder to compute $cost^H$. TAL: Tree Adder to compute $cost^L$. N : # of jobs in each machine. In : $\{K.ID, sum^H, sum^L, T_i^K\} \times N$. Out : $\{sum^H, sum^L\} \times N$. (b): **Individual Job Cost Calculator**. (c): α_j **check module**. CAM: Content Addressable Memory. $K.ID$ is used as the tag for content matching and data retrieval. (d): **Virtual Schedule Manager**.

via limited number of memory ports and would add considerable access latency, thereby severely degrading scheduler performance. To avoid the performance bottleneck, we use a fully register-based implementation of JMM as shown in Figure 5. Each register is $24 + x$ bits wide (c.f., Figure 5), where $x = \lceil \log_2(M \times N) \rceil$. Each job attribute is 8 bits wide. We discuss the rationale for selecting 8-bit wide attributes in Section 4.2.

4.1.2 Cost Calculator (CC). Figure 6a shows the μ architecture of the CC to compute scheduling cost. The inputs to the CC include the metadata of jobs currently scheduled in the machine and the weight ($J.W$) and EPT ($J.\hat{\epsilon}_i$) of the new job. The outputs of the CC are – (1) the updated values of sum^H and sum^L for all jobs in M_i , (2) the cost of assigning the new job, (3) the WSPT ratio of the new job, and (4) its index in the V_i based on WSPT ratio comparison. Additionally, the CC updates job-specific costs, sum^H and sum^L , and the index of the new job in the V_i based on the WSPT comparison. The sum^H and sum^L are stored in the JMM for future computations, and the cost and job index are forwarded to the Cost Comparator. Each machine is equipped with a CC to concurrently compute cost for a new job across all machines within a single cycle.

A key observation from Section 3.2 is that the sum^H and sum^L can be computed in parallel. To exploit this parallelism, the CC includes up to N instances of *Individual Job Cost Calculator* (c.f., Section 4.1.3). We choose *Tree Adders* to minimize computation latency by enabling single-cycle summation. Each Tree Adder consists of $N - 1$ adders arranged in $\log_2 N$ stages. Although an accumulator-based design would reduce area, it would require multiple cycles per computation,

thus degrading scheduler performance. The Tree Adder provides an optimal trade-off between the scheduler performance and hardware cost. We use two Tree Adders per CC, one for sum^H (TAH) and another for sum^L (TAL). We multiply output of TAH by the weight of new job to compute $cost^H$ and output of TAL by the expected processing time of new job to compute $cost^L$. The **Job Index Calculator** acts as a popcount [27] to compute the number of 1's in its input.

4.1.3 Individual Job Cost Calculator (IJCC). Figure 6b shows the μ architecture of the IJCC. Each job in V_i contributes either to the $cost^H$ or the $cost^L$ based on its WSPT classification relative to the new job (c.f., Section 3.1). However, the IJCC computes both $cost^H$ and $cost^L$ and masks out irrelevant cost term as needed. Specifically, the $cost^H$ output is zero (**0**) if *either* the new job has an invalid ID (i.e., no job is present), *or* the WSPT of the job under consideration is lower than that of the new job. Similarly, $cost^L$ is set to zero (**0**) if the WSPT of the job under consideration is greater than that of the new job. Incorporating this decision logic within the IJCC eliminates the need for additional job-specific condition checks from CC and propagation of job attributes to other scheduler components, reducing routing congestion and resource utilization while improving scheduler performance. Additionally, IJCC computes sum^H and sum^L . The job at the head of V_i performs VW , requiring modification of its attributes. To enforce this, each job's ID is compared with the ID of the job at $Head.V_i$. If the IDs match, the updated values are written back to the JMM. Otherwise, the original values are preserved. The output of the WSPT comparator is **1** when $T_i^K \geq T_i^J$ and is forwarded to the Job Index Calculator.

4.1.4 Memory Management Unit (MMU). The primary function of the MMU is to manage access to the JMM. MMU acts as a bridge between Phase II and Phase III of the scheduler aiding each scheduler component to access necessary job metadata information quickly. A dedicated MMU helps to write the new job metadata quickly at a free JMM location instead of time-consuming search. MMU maintains two data structures – (1) a lookup table (LUT) that maps each Job ID to its metadata address and (2) a FIFO of free memory addresses. The LUT is used during metadata invalidation. A Job's metadata is discarded upon receiving an invalidate signal from the α_J Check and its address is queued in the FIFO for future use. When a new job is scheduled, the CC requests a free metadata address from the MMU. The MMU responds by popping an available address from the FIFO and returning it to the CC.

4.1.5 Cost Comparator (CR). The CR compares the costs across machines and sends the new job's ID and its index in V_i to α_J check module. The CR also informs the CC of the machine selected, which in turn interacts with the MMU to find the next available memory address and pass this information on to JMM to store the new job's metadata.

4.1.6 α_J Check (AC). Figure 6c shows the architecture of the α_J check module. AC tracks the amount of time (calculated as $t = \alpha_J \cdot \hat{\epsilon}_i$) a job J spends at $Head.V_i$ and decrements it by one (**1**) every clock cycle. Once the counter reaches zero (**0**), the job is popped from the Virtual Schedule Manager (VSM) and sent to the designated machine. The AC consists of a Content Addressable Memory (CAM) of size N with job IDs as the tag and t as the content. When a job is popped from the CAM, the corresponding entry is invalidated in the MMU and the job is also popped from VSM. Intuitively, using a CAM enables to dynamically reorder the jobs as per the WSPT values with minimal computational overhead. Note, a new job J may replace the job at $Head.V_i$ if J 's WSPT is higher than that of the head job, requiring a job reordering.

4.1.7 Virtual Schedule Manager (VSM). Figure 6d shows the architecture of the VSM which maintains the ordered list of jobs scheduled on a given machine. On receiving a pop from AC, VSM releases the head job to the designated machine. We use a configurable shift-register structure,

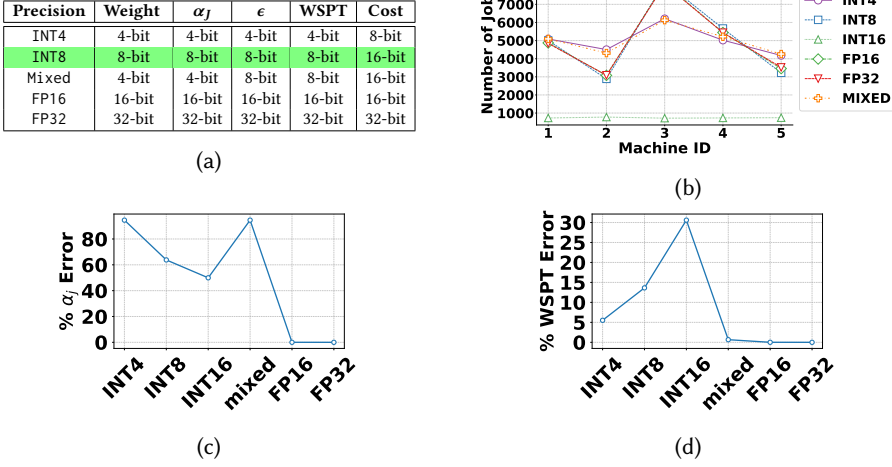


Fig. 7. (a): Various quantization techniques applied to each job attribute to evaluate effect of quantization on final schedule computation. Green highlights the most suitable quantization. (b): Scheduled job distribution in each machine. (c): % Error in α_J . (d): % Error in WSPT.

where each register stores the Job ID ($J.ID$) of one scheduled job and supports left shifts, right shifts, and partial shifts, enabling dynamic reordering based on job's arrival and departure. The VSM updates either (a) when a job is released to the machine (departure) or (b) is assigned to the machine (arrival). Note, arrival and departure may occur at the same time. The maximum capacity of VSM is N . The job at index k is referred to as J_k , $k \in [0, N - 1]$ and J_0 represents the job at $Head.V_i$. When a job is released, all remaining jobs are right-shifted to preserve job ordering such that $J_{k-1} \leftarrow J_k$. When a new job is scheduled, it can be inserted at any index $p \in [0, N - 1]$. To accommodate the new job at position p , jobs from J_p to J_{N-2} are shifted left by one position (i.e., $J_{p+1} \leftarrow J_p$), while entries before p remain unchanged. The register at index p is then updated with the new Job ID. A full left shift occurs when $p = 0$ (i.e., when WSPT of J_0 is lower than the WSPT of new job), and a partial left shift is performed when $p > 0$.

To implement this behavior, each register is connected to a *Data Selector* (DS) which chooses one of four inputs – the job ID from the left or right neighbor, the new job, or the current value (no change). The DS receives the job Index from CC and the pop signal from AC. Based on these inputs, DS generates a control signal for each register to perform the appropriate update. The ID of the job at $Head.V_i$ is shared with both AC and CC to coordinate α_J point tracking and cost computation.

4.2 Quantization Selection Rationale

The SOS algorithm contains complex mathematical operations that can degrade scheduler performance (e.g., increased dynamic power at a higher job arrival rate) if done at full floating-point precision (i.e., at FP64). To ensure that the scheduler exhibits high performance (i.e., scheduling job in near real time) while minimizing area and power consumption, the SOS algorithm requires us to operate with reduced numerical precision with modest reduction in scheduling accuracy. To identify an appropriate numerical precision, we evaluate SOS algorithm using various numerical precision detailed in Figure 7a.

We choose five different machine configurations and varying workload (c.f., **Workload generation** in Section 7 for details) to empirically identify the suitable numerical precision. We set the

minimum job weight to one (1), and the minimum expected processing time to 10. We choose SOS algorithm's performance at FP32 as the baseline for identifying the suitable numerical precision for the scheduler. Figure 7b shows that INT8 quantization closely replicates the FP32 job distribution. Additionally, we analyzed errors in key job attributes. According to Equations (4) and (5), cost accuracy is only influenced by the jobs currently scheduled on a machine. Hence, errors in a Job's WSPT and α_J can significantly impact scheduling decisions. Figures 7c and 7d present the error in WSPT and α_J , respectively. INT8 exhibits the second-highest WSPT error, while INT4 and Mixed-precision approaches show lower WSPT errors. However, INT8 demonstrates lower α_J error than INT4 and Mixed quantization. Consequently, the latter schemes release jobs for execution earlier than intended, resulting in erroneous cost calculation and increased cost error. ***These observations form the basis for choosing INT8 as our preferred precision level.***

5 Systemic Bottlenecks in HERCULES μ Architecture

We will now re-explore design and implementation of HERCULES and correlate different design decisions to various performance bottlenecks. Our primary bottleneck concerns relate to the maximum system size HERCULES could support, which was capped at 10 machines. Similarly, while HERCULES vastly outperforms a software SOS implementation, individual scheduling took 466 cycles (c.f., Section 8.3). While iterations can overlap, this is still a significant delay to an individual job being assigned to a machine. In doing this, we will identify elements of operation and instantiation that need to be enhanced and/or augmented to create an improved scheduling accelerator architecture.

Memory Interface: The memory interface of HERCULES, used to read in job metadata for scheduling and writing out resultant schedules, operates by sending over batches of X number of jobs at a time, and then returning the information for those X jobs when all of them are completed. This was useful for timing of releases on the scheduler's end, and allowed us to track individual jobs closely throughout their processing. However, this batching method imposes severe overheads on the scheduling operation – while waiting for new jobs, we are waiting for the host to read and organize X jobs at a time, delaying their initial arrival. This method also imposes a hardware overhead in the form of requiring the FPGA to write and track a table X entries long, where any arbitrary machine needs to be able to write popped jobs to any arbitrary entry in that table, which then needs to be sent over in one go. This imposes both a resource utilization overhead as we need to track extra information across cycles, but also affects scalability, as each new machine in the configuration increases the number of components that need to be routed to this table.

Iterative Cost Comparator: In HERCULES the calculated costs for each machine are compared in an iterative, sequential manner. This imposes some control overhead, but more importantly also imposes direct iteration latency costs that correspond to the scaling of the configuration, as this comparison operation is computationally bounded by $O(N)$, N : Number of machines.

Redundant Circuitry in Cost Calculator: In HERCULES, the cost calculation has been vastly simplified over the theoretical basis, making it much more amenable to hardware acceleration. However, in the design of HERCULES, our goal was to streamline the overall pipeline of assigning a given task to a machine. As such we used CAM for the job metadata that was fully sent over to the cost calculator. The cost calculator performed every possible calculation for each job. The memory management unit then had to select which computations were actively being kept, depending on the ordering of the jobs, whether they were receiving virtual work, and whether they were still valid within the schedule. As such, the Cost Calculators in HERCULES were filled with redundant circuitry and needed to wait on multiple components to achieve coherency before the final cost

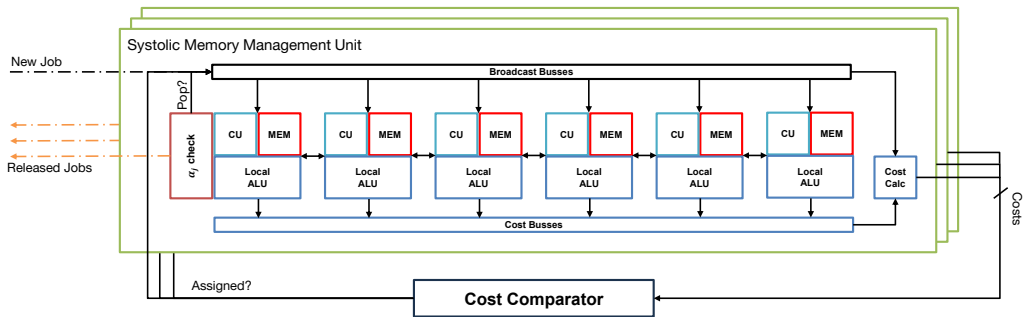


Fig. 8. **The Systolic SOS μ architecture, as used in STANNIC.** This architecture places maintaining the order of the Virtual Schedules as the primary function of scheduling. To do so, it uses one dimensional systolic arrays that track each individual job, and leverages the ordered nature of the virtual schedules to enhance the performance of other functionalities.

was accurate. This imposes severe latency and resource cost penalties, contributing to HERCULES's 466 cycle iteration.

Decentralized Memory Management: In HERCULES, to facilitate the job assignment, the responsibility of tracking distinct attributes of the Virtual Schedules for each machine was split into three distinct components. The JMM tracks the associated attributes of any given job that are required for the cost calculations. The VSM tracks and maintains the WSPT ordering of jobs within a given Virtual Schedule, inserting and removing jobs as needed. Lastly the MMU enforces coherency between the other two elements, ensuring Virtual Schedule Manager knows when changes to the schedule are required, and so the Job Metadata Memory knows which job values need to be updated or marked invalid based on updates in the Virtual Schedule. The *time required for these discrete components to achieve coherency imposes a delay on iteration speed and the intense intercommunication between each of these elements imposes significant routing congestion*. By requiring each of these components to be capable of full intercommunication about arbitrarily ordered data, each component requires dense interconnectivity, leading to routing for designs tracking more than 10 machines to fail using the HERCULES architecture. Consequently, we identify this decentralized memory management system as the crucial bottleneck on system scalability in HERCULES.

6 STANNIC: Virtual Schedule-Centric Hardware Implementation of SOS

In this section, we present a systolic-array-based SOSA called STANNIC to alleviate the limitations of HERCULES as detailed in Section 5. We discuss the primary subcomponents, and establish their functional parity with components within the HERCULES SOSA. In doing so, we establish a high-level functional similarity of the two architectures, while also clarifying how the difference in organization (and core model) results in a centralized design with improved scheduling performance and hardware resource usage.

6.1 Systolic Architecture for STANNIC

In this section, we describe the μ architecture of STANNIC in detail. Figure 8 shows the entire block diagram of the STANNIC μ architecture.

6.1.1 Systolic Memory Management Unit (SMMU). STANNIC reorganizes and unifies each machine's individual scheduler functionality within a set of Systolic Memory Management Units (SMMUs).

A SMMU is dedicated to each machine in the corresponding system we are scheduling for. The SMMU primarily consists of a one-dimensional systolic array, which tracks the corresponding machine M_i 's virtual schedule V_i across each of its **PEs**. Each PE represents an index in the V_i , and is responsible for both moving and updating cost metadata for job K while it is in that index. Each SMMU also contains a **Cost Calculator** that performs necessary computations for the final cost calculation when a new job is considered. Lastly, the SMMU contains two busses, one to broadcast metadata (**Broadcast Bus**) of a new incoming job J to each PE for local WSPT comparison, and the other to send the cost sub-components to the Cost Calculator (**Cost Bus**).

6.1.2 Processing Element (PE). Each PE contains the logic and memory necessary to independently track a single job K and its associated cost attributes. **Memory (MEM)** stores job metadata, such as α_J point, T_i^K , $K.ID$, $n_K(t_C)$ (where t_C is the current cycle), as well as local pre-calculated sum_K^{HI} and sum_K^{LO} values as mentioned in Sections 3.2 and 3.3. Across iterations, these precalculations are updated in the **Local Arithmetic Logic Unit (Local ALU)**, with the exact mathematics detailed in Section 6.2. Lastly, the **Control Unit (CU)** collects global and local signals from the broadcast bus and neighboring PEs, respectively. These signals are decoded to determine local data movements and arithmetic updates as required to maintain the WSPT ordering of the overarching V_i .

The **Head PE**, which corresponds to $Head.V_i$, differs from the rest of the PEs in that it includes the α_J **check** module and has a modified CU. The α_J check module checks whether $n_{Head.V_i}(t_C) \geq (\alpha_J \times Head.V_i.\hat{\epsilon}_i)$, and thus should be released from the schedule. When this happens, it sends a pop signal across the SMMU's broadcast bus, alerting all other PEs of the coming change. The CU is modified to account for the fact that the Head PE has no left neighbor, and thus requires different control logic to ensure proper job insertions. This is not necessary for the tail, as job insertions can only occur into V_i 's which have space, and thus have an invalid job in their tail PE.

6.1.3 Cost Comparator (CC). The CC is the only module that is separate from the SMMU. It is a singular shared module that receives all of the individual machine costs calculated by the SMMUs. This is necessary to complete the inter-machine scheduling phase (**Phase II**) of the SOS algorithm. This is done with an iterative comparator, like in HERCULES.

6.1.4 Architectural Similarities Between HERCULES and STANNIC. The STANNIC architecture achieves the same functional requirements as HERCULES by consolidating the decentralized components into the centralized SMMU with its systolic array V_i . We show a component mapping between the two architectures in Table 1.

This architectural shift moves the responsibility of memory management and WSPT ordering maintenance from three discrete, intercommunicating components to the local decision making of PEs in a Centralized Systolic Array structure. This design choice leads to significant reduction in routing congestion and iteration latency due to communication overheads. In Section 8, we will show that the STANNIC architecture results in an average $7.5\times$ iteration speedup and a $14\times$ increase in maximum routeable system configuration size as compared to HERCULES.

HERCULES	STANNIC
Memory Management Unit	Systolic Memory Management Unit
α_J check	α_J check (head only)
Virtual Schedule Manager	Control Unit
Cost Calculator	Local ALUs, Cost Calc
Job Metadata Memory	MEM
Cost Comparator	Cost Comparator

Table 1. Mapping between the architectural components of HERCULES and STANNIC. This correspondence establishes similarities between the high-level abstract responsibilities of individual components, but the actual methodologies implemented to perform those responsibilities differ across the two architectures.

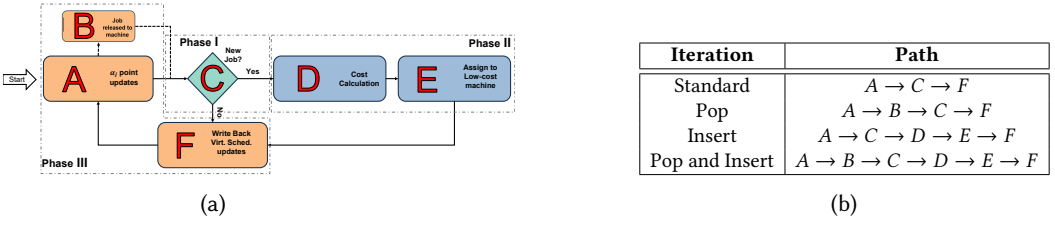


Fig. 9. (a): **Annotated Algorithmic Flow** derived from Figure 2b with additional annotations. (b): **Iteration Mapping** showing the four paths through (a), classifying each as a specific type of iteration.

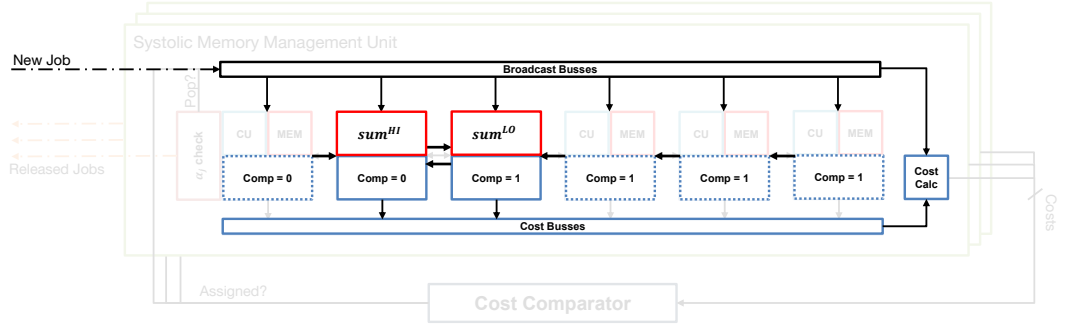


Fig. 10. **An illustrative example of cost calculation within the systolic virtual schedule architecture.** Each PE is capable of performing a local WSPT comparison, self identifying which set they are in. By then looking at the direct neighboring PEs, local elements can self identify as threshold elements, and thus contribute a memoized summation of all lower/higher costs as needed, removing the summation iteration latency and improving overall speed.

6.2 Systolic SOS Operation

Using our Virtual-Schedule based perspective on the SOS algorithm (c.f., Figure 2b), we can see that the algorithm has four looping paths (Figure 9b), but each returns us back to the start point of the scheduling iteration. The operational efficiency of STANNIC relies on maintaining an *ordered* V_i in our systolic array as a fundamental loop invariant. The systolic array enables parallelism by allowing each PE to use this ordering and local data to accelerate cost calculation and maintain state coherence with minimal routing overhead. By Definition 3, a V_i 's ordering is done by WSPT ratio ranking. We will expand upon this to define *Properly Ordered Systolic Virtual Schedule*.

Definition 4. Properly Ordered Systolic Virtual Schedule: A Virtual Schedule V_i , tracked by a systolic array, is properly ordered if:

- The **Head PE** (PE_0) is either empty or contains the job $K, K \in V_i$ with the highest WSPT ratio T_i^K of all jobs in the virtual schedule.
- For any valid job K in PE_i , the neighbor to its immediate "right" (PE_{i+1}) contains either a job K_R with $T_i^{K_R} \leq T_i^K$, or an invalid job.
- There are no invalid jobs (bubbles) between two PEs that contain valid jobs.

6.2.1 Systolic Cost Calculation. STANNIC accelerates cost calculation by leveraging the ordered systolic V_i to precalculate and memorize the summation terms sum^{HI} and sum^{LO} (c.f., Equations (4) and (5)). Figure 10 illustrates an example of how the systolic V_i contributes to cost calculation.

As detailed in Section 3, the cost of assigning a new job J onto machine M_i is calculated using two discretized terms, $cost^H$ and $cost^L$. Individual jobs $K \in V_i$ contribute to one of these two terms based on the WSPT of job K to the new incoming job J . As such, upon the arrival J , its WSPT T_i^J is broadcast to all PEs. Each PE, tracking job K with WSPT T_i^K , performs a local comparison C :

$$C = \begin{cases} 0, & \text{if } T_i^K \geq T_i^J \\ 1, & \text{otherwise} \end{cases} \quad (6)$$

A comparison value of $C = 0$ indicates that job K contributes to sum^{HI} , whereas a value of $C = 1$ indicates that job K contributes to sum^{LO} for the cost calculation of job J . Note that $C = 1$ even when a PE is not tracking a valid job. As such, assuming the invariant of a properly ordered systolic V_i as defined in Definition 4, reading the comparison values C from the Head PE to the Tail PE results in a string of zeros followed by a string of ones.

This means the *comparison threshold* between the two cost sets for sum^{HI} and sum^{LO} can be found between two PEs: the last PE with $C = 0$, and the first PE with $C = 1$. After each PE has calculated its own comparison value C , it can then check the comparison values of its neighboring PEs, and self-identify as part of the threshold. We notate a PE's neighbors comparison values as C_R and C_L for the right and left neighbor, respectively. As noted in Section 6.1.2, each PE contains two local memorized values: sum_K^{HI} and sum_K^{LO} . sum_K^{HI} computes if the PE's tracked job K were the last element in the higher priority set, whereas sum_K^{LO} computes if the PE's tracked job K were the first element in the lower priority set. Initial calculation and maintenance of sum_K^{HI} and sum_K^{LO} is discussed in Section 6.2.2. During cost calculation, instead of iteratively summing over the individual contributions in the systolic array, the two PEs at the threshold can self-identify and volunteer their memorized values to the Cost Calculator. The PE with local $C = 0$ contributes its sum_K^{HI} for the calculation of $cost^H$, while the PE with local $C = 1$ contributes its sum_K^{LO} for the calculation of $cost^L$. In doing this, we entirely remove the latency associated with summation across the depth of V_i , converting the summation into a single-cycle lookup operation.

6.2.2 Maintaining Virtual Schedule Ordering. To accurately perform cost calculation, we need to maintain the proper ordering of the virtual schedule V_i as a loop invariant across iterations of the algorithmic flow (c.f., Figure 9). Maintaining this loop invariant can be done with local, and thus parallel, PE decisions and updates by individual PEs in response to global signals. There are four categories of iteration through the algorithmic flow, each of which requires different actions in order to maintain the loop invariant.

- (1) **Standard Iteration.** A standard iteration occurs when no new job has been assigned to machine M_i , and the job at $Head.V_i$ has not yet reached its α_J release point. In a standard iteration, schedule ordering remains stationary but the memorized cost values across the systolic array need updating to reflect the accrual of Virtual Work for $Head.V_i$. The operation of a standard iteration proceeds in parallel across the array, and is illustrated in Figure 11. There are two PE actions – (a) **Head PE Action:** The Local ALU updates both sum_K^{HI} and sum_K^{LO} by decrementing them. sum_K^{HI} is decremented by 1, and sum_K^{LO} is decremented by T_i^K representing one cycle of completed Virtual Work as described in Section 3.3; and (b) **Subsequent PE Action:** Every other PE that is currently tracking a valid job has a job K that by definition has a lower or equal WSPT than the job at $Head.V_i$. As such, their local sum_K^{HI} represents a summation that includes $sum_{Head.V_i}^{HI}$. The local ALUs in the other PEs must therefore also decrement the local sum_K^{HI} by one. sum_K^{LO} remains unchanged. Each PE's CU selects its own Local ALU as the source for memory write-back. This operation maintains the WSPT order while ensuring that

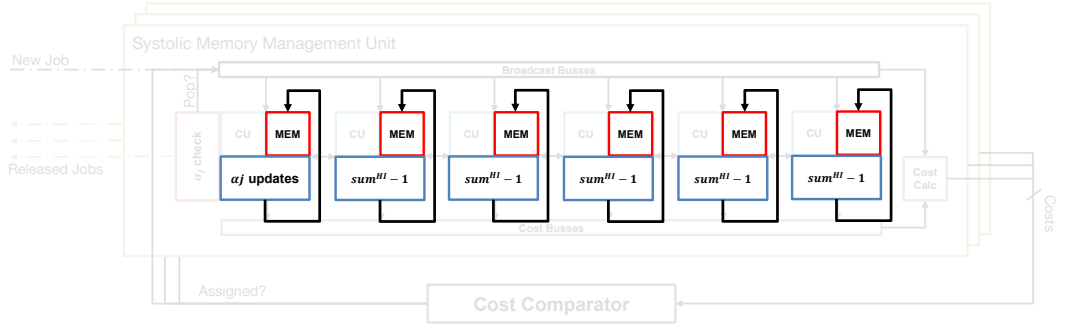


Fig. 11. **Standard Iteration updates and writeback paths.** Local memoized cost updates are written back directly to local memory α_j updates: At the head, it performs the same incremental updates as described in part two of Section 3.3. Each other job only needs to perform the updates to sum^{HI} as the job in the head PE is by definition in the set of jobs with a higher WSPT than themselves.

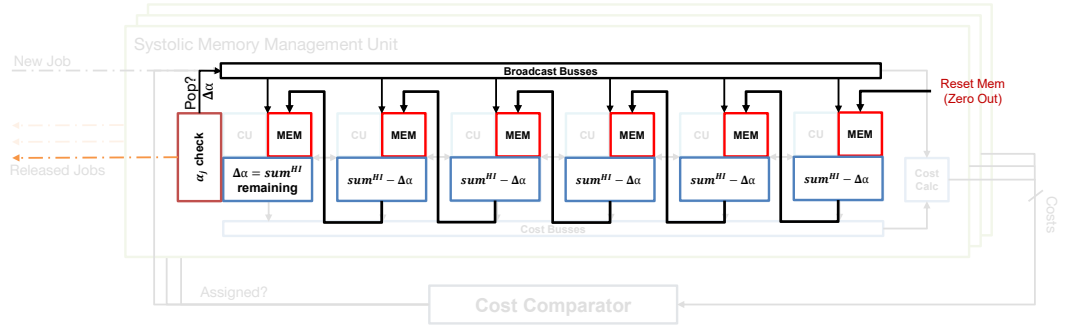


Fig. 12. **POP Iteration updates and writeback paths.** The head PE recognizes that its current job has reached its α_j point, and as such notifies the relevant machine queue to finalize scheduling. The rest of the jobs are still in order, but simply clearing head would insert a “bubble” which would break proper ordering definition. Instead, each PE calculates the new sum^{HI} value of their given job to account for the head job leaving, and then the CU selects the ALU of the right neighbor as the source of the local memory writeback. The tail “inserts” an invalid job at the end.

all memorized cost values accurately reflect the virtual work completed by the highest priority job.

- (2) **POP Iteration.** A POP iteration occurs when the job in the Head PE has reached its α_j release point, requiring that job to be released to the machine’s work queue, removing it from the V_i . The goal is to remove the job from the Head PE, and shift all subsequent jobs to the left in order to preserve the WSPT ordering and maintain the no-bubbles element of our invariant. The process of doing this is illustrated in Figure 12. POP iteration has three different types of iterations – (a) **Job Release and Broadcast:** This iteration starts with the α_j check module identifying that the $Head.V_i$ job has reached its release point. It releases the job’s ID to the work queue, and simultaneously broadcasts both a pop flag and the remaining value $\Delta\alpha = sum^{HI}_{Head.V_i}$. This value represents the remaining contribution of the current job at $Head.V_i$ to all the other jobs $K \in V_i$ ’s sum^{HI}_K ; (b) **Cost Updates:** Each PE performs the subtraction $sum^{HI}_K - \Delta\alpha$ in their Local ALU. This subtraction is necessary as $Head.V_i$ is now being removed from the set and

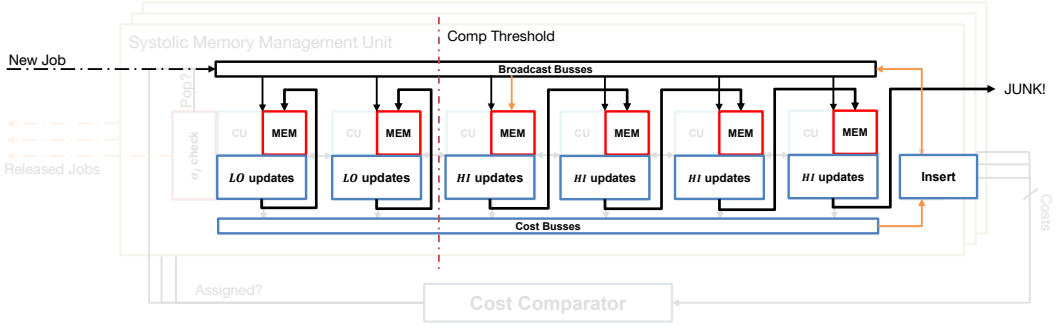


Fig. 13. **Insert Iteration updates and writeback paths.** Job insertion implies that cost calculation comparisons have been performed in this cycle for the current jobs already. These local comparisons can be reused to recognize which of two categories a given job is in. **HI set:** All jobs with a higher WSPT than the new job. They perform the standard α_j updates, but additionally add the low cost of the new job to their sum^{LO} as it will be inserted below them. **LO set:** All jobs with a lower WSPT instead account for the new job in their sum^{HI} total. Additionally, to make space for the new job each PE in this set writes the new data from their left neighbor, except the PE at the threshold, which instead writes the data associated with the new job, whose initial sum^{HI} and sum^{LO} values are calculated in the cost calculator.

PE Set	Comparison Value C	Reordering Action	Cost Updates
HI Set	$C = 0$	Stationary	$sum_K^{LO} + J.W$
LO Set	$C = 1$	Synchronous Right-Shift	$sum_K^{HI} + J.\hat{\epsilon}_i$
New Job J	$C = 1, C_L = 0$	Stores New Job	Loads Initial sum_J^{HI} and sum_J^{LO*}

Table 2. **Insert Iteration Behavior for different sets of PEs.** Each PE can identify which set they are a part of using C and C_L . *The initial memoized costs for J are calculated in the overall cost calculator. The PE that will store job J still needs to calculate $sum_K^{HI} + J.\hat{\epsilon}_i$, so that the next PE can store this updated value during the right-shift.

should not be considered for any subsequent cost calculations; and (c) **Synchronous Left-Shift:** Lastly, in the write-back stage of this iteration, each PE synchronously writes back the data from its right neighbors ALU (i.e., $PE_i \leftarrow PE_{i+1}$). The tail's right neighbor ALU inputs are hardwired to zero, in essence resetting the memory and inserting an invalid job at the end of the virtual schedule. This maintains proper ordering while simultaneously removing the released job from the schedule and any memorized cost components.

- (3) **Insert Iteration.** An Insert iteration occurs when the machine corresponding with a particular Virtual Schedule V_i has been selected as the minimum-cost machine for a new job J . At this point, the V_i must reorder itself to insert J in the correct WSPT ordering position. Additionally, new memorized costs need to be calculated for J and all other jobs need to update their local cost to account for the new job now being present in either their sum_K^{HI} or sum_K^{LO} set. An illustrated example can be seen in Figure 13, while Table 2 shows the three distinct sets of behaviors. The selection of machine M_i as the lowest cost machine implies that a cost calculation has been performed earlier in this iteration (c.f., Section 6.2.1). As such, each PE still has a local comparison value (C) to self-identify as part of the high or low WSPT set, relative to the new job J . Furthermore, by checking the C value of a neighbor, the threshold between these two sets can be locally self-identified by PEs as well. We can use this information to inform a specific PEs

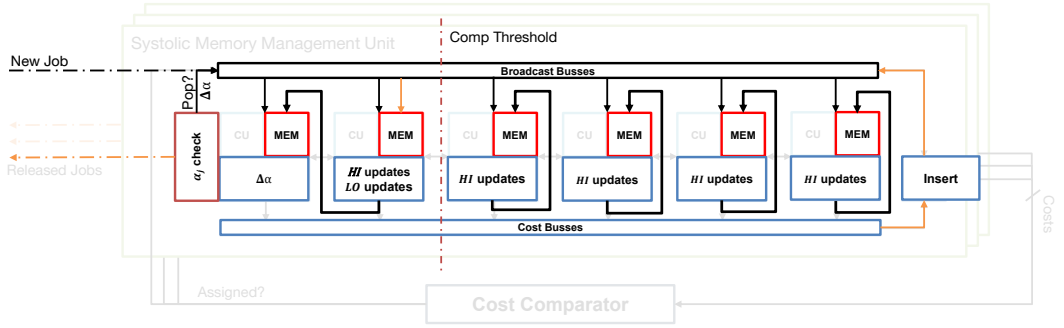


Fig. 14. **POP and Insert Iteration updates and writeback paths.** In the case that a POP and insert occur in the same iteration, the two schedule reordering operations are overlapped, causing the high set to shift left and the low set to remain stationary due to effectively left and right shifting simultaneously. The new job is inserted on the left of the threshold to account for the POP's left shift. Relevant cost updates account for not only the addition of the new job, but also the subtraction of the head job's remaining cost $\Delta\alpha$.

behavior, both in terms of cost update calculation and reordering. Insertion iteration comprises three distinct computation – (a) **Cost Update Calculation:** All jobs that have a higher WSPT than J (i.e., the sum^{HI} set) need to account for the new job inserted below them, and so need to update sum_K^{LO} . All jobs in the LO set instead need to calculate an updated value of sum_K^{LO} . The initial memorized values for job J are calculated in the overall cost calculator. The cost calculator has sum^{HI} , sum^{LO} , $J.W$ and $J.\hat{\epsilon}_i$ already when performing the cost calculation, and so can calculate $sum_J^{HI} = sum^{HI} + J.\hat{\epsilon}_i$ and $sum_J^{LO} = sum^{LO} + J.W_i$ simultaneously. For each of these calculations, they happen on top of the α_J cost updates, as detailed in the Standard Iteration; (b) **Reordering:** To maintain proper ordering, J must be inserted after all the jobs in the HI set, and right before all the jobs in the LO set, with each of the jobs in both sets maintaining their current orders. As such, PEs with $C = 0$ store the values from their own ALU during write back, and most of the PEs with $C = 1$ store the information from their left neighbor. An exception to this is the PE with $C = 1$ and $C_L = 0$, which is the PE that was the low side of the comparison threshold. This PE corresponds to the index at which J needs to be inserted, and as such, it loads all of its new data from the broadcast bus; and (c) **Edge Cases – Inserting at Head PE:** When the incoming job J has a higher WSPT than all existing jobs, it must be inserted into the Head PE. Since the Head PE has no left neighbor, the Head PE's CU has different control logic that recognizes if $C = 1$, the Head PE is the insertion point. This also covers inserting J into an otherwise empty V_i . **Full V_i** if we were to try an insert a job into a full systolic array (i.e., a systolic array with a valid job in each of the PEs), the job in the tail PE would be lost, as no PE will store it during the writeback cycle. As such, full V_i s can not be assigned new jobs.

- (4) **POP and Insert Iteration.** Finally, a POP and Insert Iteration happens when the job at $Head.V_i$ reaches its α_j release point in the same iteration in which machine M_i is selected as the lowest-cost machine for an incoming job J . This iteration combines the functional requirements of the individual POP iteration and Insert iteration. Memorized cost updates need to account both for the $\Delta\alpha$ of the departing job, as well as the $J.W$ or $J.\hat{\epsilon}_i$ of the incoming job (depending on relative WSPT). Lastly the array must account for the left-shift and insertion in a single update. An illustrated example can be seen in Figure 14, with the three sets of behaviors being described in Table 3. (a) **Cost Updates:** The HI set needs to calculate updates for both of its

PE Set	Comparison Value C	Reordering Action	Cost Updates
HI Set	$C = 0$	Left-Shift	$sum_K^{LO} + J.W, sum_K^{HI} - \Delta\alpha$
LO Set	$C = 1$	Synchronous Right-Shift	$sum_K^{HI} + (J.\hat{\epsilon}_i - \Delta\alpha)$
New Job J	$C = 0, C_R = 1$	Stores New Job	Loads Initial sum_J^{HI} and sum_J^{LO*}

Table 3. **POP and Insert Iteration Behavior for different sets of PEs.** Each PE can identify which set they are a part of using C and C_R . *The initial memoized costs for J are calculated in the overall cost calculator. The PE that will store job J still needs to calculate $sum_K^{LO} + J.W, sum_K^{HI} - \Delta\alpha$, so that the previous PE can store this updated value during the left-shift.

memorized values, as the job at $Head.V_i$ is being removed from its sum_K^{HI} summation, and J is being added to its sum_K^{LO} summation. For LO set PEs, their sum_K^{HI} needs to remove $Head.V_i$ while adding J into its summation. For the initialization of sum_J^{HI} and sum_J^{LO} , the only difference compared to the Insert Iteration is that sum_J^{HI} must now also account for $Head.V_i$ leaving. As such $sum_J^{HI} = sum^{HI} + (J.\hat{\epsilon}_i - \Delta\alpha)$; (b) **Overlapped Reordering**: Rather than performing the two movements separately, they can be composed into a singular transformation. For a POP iteration, every PE shifts left. In an insert operation, the HI set remains stationary, while the LO set right shifts to create a space for job insertion. Combining these two results in a net left-shift for the HI set, and the LO set remaining stationary. To properly account for the new job being inserted and then shifted to the left, we can simply insert it one index to the left compared to a regular Insertion Iteration. This is equivalent to inserting it at the HI end of the comparison threshold (*i.e.*, the PE with $C = 0, C_R = 1$); and (c) **Edge Case – J Has Highest WSPT**: In the case that J has the highest WSPT, the Head PE would have a $C = 1$, and there would be no PE with $C = 0$ in the entirety of the V_i . However, in such a scenario, job J would have to be inserted into the Head PE anyway to maintain proper WSPT ordering. As such, when the Head PE recognizes a POP, it sets $C = 0$. This way the CU can check if $C_R = 1$ and correctly self-identify as the insertion point PE.

7 Experimental Setup

In this section, we outline the experimental setups for the evaluation of our scheduling architectures. We set up two broad categories for these evaluations. The first of these categories (outlined in Section 7.1) is the output schedule evaluation, which we use to compare the produced schedules of our accelerated algorithm to other preexisting methods. The second category (outlined in section Section 7.2) is the setup for direct architectural performance comparisons between HERCULES and STANNIC.

7.1 Output Schedule Evaluation

Target machine configurations: We have used five (5) machine configurations – **M1**: ⟨CPU, Best⟩, **M2**: ⟨CPU, Worst⟩, **M3**: ⟨Mixed, Best⟩, **M4**: ⟨GPU, Best⟩, and **M5**: ⟨GPU, Worst⟩.

Workload generation: We have developed an in-house workload generator (WG) to emulate job dispatch in heterogeneous systems with varied job distributions, reflecting real-world scenarios such as CPU-heavy/GPU-heavy bursts. The WG has multiple configurable parameters – (a) **Job Composition** (JC) captures the fraction of compute intensive, memory intensive, and mixed jobs, summing to **1.00**; (b) **Machine Composition** (MC) captures numbers of CPU/GPU/Mixed machines; (c) **Burst Factor** (BF) captures maximum number of jobs that may be released in a single clock tick; (d) **Burst Type** (BT) captures job arrival patterns. For *random*, jobs are released at randomly selected ticks and for *uniform*, a BF amount of jobs are released every tick; (e) **Idle Time** (IT)

captures number of ticks inserted after a specified number of jobs are released; and (f) **Idle Interval** (II) capture maximum number of jobs released before inserting an idle period. BF and BT model the **uncertainty** in job arrivals in realistic scenarios whereas IT and II imitate time spans where **new jobs are not created until ongoing jobs are completed**.

Baseline schedulers: We compare performance of HERCULES against four baseline scheduling algorithms – Round Robin (RR) [30], Greedy [6], Work Stealing Round Robin (WSRR), and Work Stealing Greedy (WSG) [12].

Metrics for comparison: We use four metrics for comparisons. **Fairness** measures if low-performing machines are not starved. **Load Balancing** measures equality of job distribution across machines and is computed as the Coefficient of Variation (CV) in the number of jobs assigned to a machine across scheduling intervals. Lower CV indicates better load balancing. **Latency** captures the average delay between job creation and its scheduling time. Lower latency reflects faster scheduling and results in higher system throughput.

Hardware for SOS scheduler: We have used an AMD Alveo U55C [1] as our target FPGA to implement the SOS scheduler. We used Allo/HeteroCL [3, 16] programming language to design the scheduler. The operating frequency of the scheduler is 371.47 MHz.

7.2 Architectural Comparisons

For our architectural comparison experimentation, we introduce four more metrics.

Iteration Latency: The integer number of clock cycles it takes for the accelerator to complete one iteration of the scheduling process. This metric allows us to effectively quantify operational speed.

Resource Utilization: This is the number of discrete computational elements present on the FPGA that are required to physically implement our design. This makes it a good metric for evaluating relative size, and therefore relative resource efficiency of two designs.

Maximum Rout-able Configuration Size: This number represents the largest number of discrete machines a design can track while still producing a rout-able design. This is our metric defines a designs scalability.

Power Profile: This is the average measured power usage in watts of the FPGA while the scheduler is running. This metric will help us further quantify design efficiency, as physical space is not the only resource of consequence.

7.2.1 Data Gathering Methodology. For qualitative comparison, Iteration Latency and Resource Utilization are gathered by referring to the Xilinx Vitis and Vivado toolchains `csynth` [2] reports after synthesis and implementation runs were completed on the two architectures using different system configurations. Maximum Rout-able Configuration size is measured by incrementally increasing the number of machines in the configuration by ten. The largest configuration in which the design is properly synthesized is presented as the final result.

Power Draw is measured using `xbtop`, a utility available from Xilinx to gather real time performance data on a connected FPGA. To obtain measurements, the design binary under test is first loaded onto the FPGA, and then the design is used to schedule jobs in a workload suite using the same workload generation as described in the experimental setup in Section 7.1. The Power Draw measurements could then be taken during runtime.

For the sake of direct comparison of Iteration Latency, Resource Utilization, and Power Draw, these metrics are gathered for equivalent system configurations for both HERCULES and STANNIC. The four configurations (**C1-C4**) used for comparison are 5×10 , 5×20 , 10×10 , and 10×20 , where $m \times d$ denotes a system with m machines and a per machine V_i depth of d jobs. For each of our metrics, we also consider the average across all configurations for both designs.

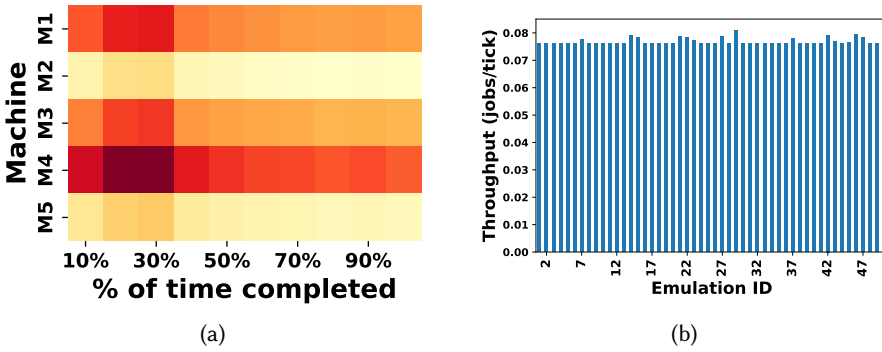


Fig. 15. (a): Average machine utilization across emulations. The darker the color, the more jobs are assigned to the machine. (b): Scheduler throughput across emulations.

8 Experimental Results

In this section, we present the results of a series of experiments using the metrics, configurations, and hardware setups described in Section 7. The first two experiments (Sections 8.1 and 8.2) demonstrate the inherent scheduling capabilities of the SOS algorithm, and the benefits of accelerating this scheduling algorithm with hardware.

Section 8.3 compares the performance and resource utilization metrics of HERCULES and STANNIC, empirically quantifying the performance improvements gained from the optimizations outlined in Section 6.2. This section presents out numeric inter-architectural comparison that corroborates the improvement claims made throughout the rest of the paper.

Section 8.4 compares the efficiency of the resulting schedules from SOSA with alternative baseline schedulers, demonstrating the benefit of using the SOS algorithm while scheduling in an online, stochastic, and heterogeneous context. Due to the two architectures implementing the same scheduling algorithm, the resulting schedules from both HERCULES and STANNIC are identical. As such, for the schedule analysis experiments of Sections 8.1 and 8.4, we present one scheduling result for the SOS algorithm.

8.1 Effectiveness of SOSA On Varying Workloads

In this experiment, we explore the effectiveness of SOSA in terms of *fairness* and *load balancing*. Toward that, we have generated 50 different workloads by varying the workload parameters (c.f., Section 7) using a Monte-Carlo simulation and then use our hardware based schedulers to schedule jobs on M1-M5 for all 50 workloads. In Figure 15a, we show the average number of jobs assigned to each machine over all 50 workloads at different fraction of time points during their run. We observe that machines M1, M3, and M4 consistently exhibit high utilization as they are best performing machines. However, despite their higher capability, the scheduler intelligently identifies when these machines reach their scheduling capacity and assign jobs dynamically to the remaining two low-performing machines, *i.e.*, M3 and M5, preventing them from starving. *Due to such intelligent scheduling, the throughput (measured in terms of jobs scheduled per clock tick) of the scheduler almost remains constant across all the 50 workloads as shown in Figure 15b.* This observation indicates that SOSA is highly capable of load balancing while maintaining high throughput and utilization of the available heterogeneous computing resources. Additionally, Figure 16a shows that M1, M3, and M4 exhibit lowest average latency as expected since they are high performance machines. This experiment shows that **SOSA is robust, adaptable to varying**

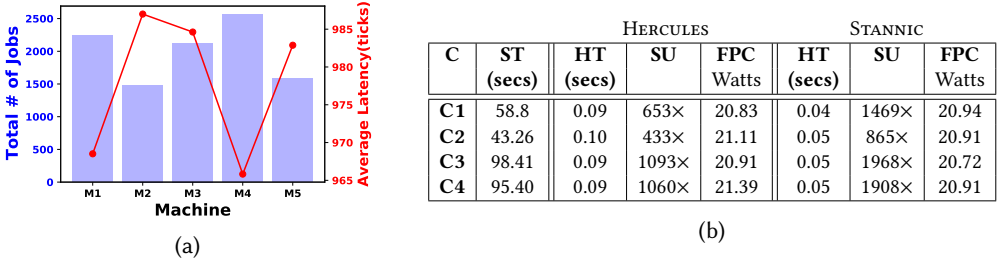


Fig. 16. (a): **Jobs and average latency per machine.** (b): **SOSA vs. software implementation.** **M**: No. of machines. **JP**: Jobs/machine. **ST**: Software execution time. **HT**: Hardware execution time. **SU**: Speedup. **FPC**: Power consumption. Here we see that STANNIC offers nearly double the speedup of HERCULES with similar power draw.

workload without compromising performance all the while ensuring high utilization of the available resources making it a prime candidate for scheduling in systems containing a plethora of heterogeneous computing resources.

8.2 Speedup Compared to Software Implementation

We compare the execution time of the SOSA with a single-threaded C implementation (SOSC) of the SOS on an Intel Xeon® W5-3433 processor running at 4.00 GHz with 512GB RAM. We consider up to 10 machines of varying capabilities (such as **M1**, **M2**, etc.), up to 20 jobs per V_i , and 10,000 jobs to schedule as shown in Figure 16b. The SOSC took up to 98.41 seconds to schedule, whereas HERCULES and STANNIC took only up to 0.10 and 0.05 seconds to schedule all the jobs, achieving a speedup of up to 1060× and 1968× respectively. Both of these architectures achieve this while consuming only up to 21 Watts of power. This experiment shows that *a dedicated hardware accelerator-based scheduler can efficiently and effectively schedule jobs on-the-fly within an acceptable power envelope.*

8.3 Architectural Comparison Evaluation

8.3.1 Iteration Latency. Figure 17a shows the recorded Iteration Latencies of the four comparison configurations, as well as their average. The average for HERCULES was 466 cycles, while STANNIC's was 62 cycles. This means that *on average the STANNIC architecture has a 7.5 times reduction in latency* compared to HERCULES. It is also important to notice that where the latency of HERCULES significantly increases with the increased depth of the Virtual Schedules, STANNIC's latency is negligibly impacted. Additionally, in HERCULES, the latency increase for each machine added (with the same Virtual Schedule depth) was ≈ 7 cycles per machine, whereas for STANNIC the latency cost of a new machine was only ≈ 5 cycles per machine. This shows that not only does STANNIC reduce iteration latency across the tested configurations, its latency also increases slower with scaling when compared to HERCULES.

8.3.2 Resource Efficiency. Figure 17c shows the recorded Look Up Table Utilization, and Figure 17b shows the recorded Flip Flop Utilization of the four comparison configurations, as well as their averages. Across all configurations in both designs, the LUT usage was higher than the FF usage, but the exact utilization in both designs corresponded directly with the configuration size the recording represents. This makes sense, as this scaling in configuration will directly result in the need for more corresponding hardware to perform the virtual schedule tracking/cost calculation processes for each machine. On average across the tested configurations, HERCULES used 218,762

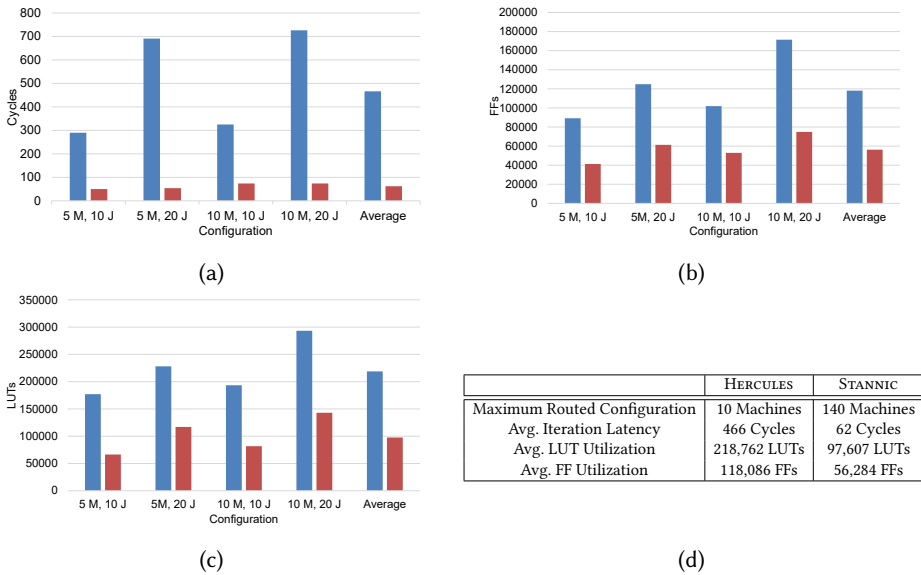


Fig. 17. **Quantitative Comparison Results** for HERCULES (blue) and STANNIC (red). All results are from synthesis runs using Xilinx tools. Average values from Figures 17a, 17b and 17c reported in Figure 17d.

LUTs and 118,086 FFs, while STANNIC used 97,607 LUTs and 56,284 FFs. This correlates to a 2.24 times reduction and 2.1 times reduction in LUT and FF utilization, respectively. As such we can see that STANNIC uses less than half of the hardware resources that HERCULES would require for an equivalent configuration.

8.3.3 Maximum Routing Configuration and Power Usage. Using the progressive configuration scaling until routing failure as described in the Section 7.2, HERCULES was capable of fully routing at a configuration size of 10 machines. STANNIC was capable of routing for a configuration of 140 machines. These results are recorded in Figure 17d, and shows a 14 times increase in scalability between the two designs. This scalability is in part due to the speedups and resource efficiency described in the last two subsections, but is primarily due to the reduced inter-connectivity routing needs that stem from the local systolic operation of schedule maintenance.

The recorded power utilization for **all** configurations across both designs can be found in Figure 16b, which shows a consistent power usage of $\approx 20.5W$. Note that while not presented in these figures, this power draw holds for the 140 Machine configuration implementation of STANNIC. As such, the FPGA's power draw was also measured in an idle state with no bitstream loaded, and that measured negligibly lower. This shows that both HERCULES and STANNIC are both power efficient designs, barely bringing the Alveo U55C above its idle power draw.

8.3.4 Summary of Comparison Results. In quantitatively comparing the two designs, we can see that STANNIC has on average a 7.5 times reduction in iteration latency and utilizes less than half the hardware resources of HERCULES for equivalent system configurations. STANNIC is also capable of scaling to schedule for systems that are 14 times larger than HERCULES was capable of. STANNIC achieves all of this while still maintaining the low power utilization of HERCULES.

8.4 Comparison of Hardware-Accelerated SOSA and Baseline Scheduling Algorithms

In these experiments, we compare SOSA against four baseline algorithms under varied workloads in terms of average latency and total number of jobs assigned to each machine **M1 - M5**.

① **Performance under evenly distributed workload:** We generate an evenly distributed workload consisting of 35% memory-intensive jobs, 35% compute-intensive jobs, and 30% mixed-type jobs. From Figures 18a, 18b, 18c, 18d and 18e, we observe that SOSA demonstrates superior performance in terms of fairness and load balancing targeting heterogeneous systems. However, SOSA exhibits slightly higher latency compared to other baseline methods as SOSA schedules by controlling the job ordering through WSPT ratio. Use of WSPT ratio helps in scheduling jobs with higher WSPT earlier, whereas lower WSPT ratio will have a higher latency.

② **Performance under memory-skewed workload:** In this experiment, we generate memory-skewed workload consisting of 70% memory-intensive jobs, 10% compute-intensive jobs, and 20% mixed-type jobs. From Figures 18f, 18g, 18h, 18i and 18j, we observe that SOSA outperforms all other schedulers in terms of fairness and load balancing implying that SOSA maintains its efficiency and decision-making consistency under significant job distribution skew. This robustness is due to its cost function, which solely relies on job weights and EPTs, allowing it to adapt dynamically to varying workloads without requiring explicit workload profiling. These findings validate that SOSA is equally effective under memory-skewed workload and can achieve high performance in real-world scenarios with significant load variations.

③ **Performance under compute-skewed workload:** We generate compute-skewed workload consisting of 70% compute-intensive jobs, 10% memory-intensive jobs, and 30% mixed jobs. From Figures 18k, 18l, 18m, 18n and 18o we observe that SOSA adapts equally well to compute-skewed workload, validating the effectiveness of SOSA's scheduling.

④ **Performance under homogeneous workload:** We generate a memory-intensive job workload. The objective is to evaluate whether SOSA maintains consistent performance targeting heterogeneous machines under a fully homogeneous workload. From Figures 18p, 18q, 18r, 18s and 18t we observe that SOSA does not outperform WSRR and WSG in terms of latency. However, SOSA, WSRR, and WSG assign a nearly identical number of jobs to each machine. FIFO-based schedulers (Greedy, WSRR, WSG) dispatch jobs in arrival order, whereas SOSA uses WSPT-based prioritization. As a result, SOSA introduces controlled delays to favor jobs with higher scheduling priority, which may increase average latency while still minimizing the weighted expected completion time. *The higher latency is not a symptom of inefficiency but a side effect of intelligent scheduling prioritization.* Furthermore, SOSA deliberately buffers jobs internally to prevent overloading machine queues – an effect not reflected in baseline scheduling algorithms. Therefore, although latency may appear higher, SOSA optimizes performance under job homogeneity.

⑤ **Performance on homogeneous machines:** We generate a compute-intensive job workload and consider only one type of target machine (CPU) with varying quality. Although SOSA is designed for heterogeneous systems, it is important to evaluate its performance for homogeneous systems, which may occur in practical deployments. From Figures 18u, 18v, 18w, 18x and 18y we observe that SOSA does not outperform the WSRR and WSG in terms of latency for its WSPT-based scheduling. However, job distribution across machines is nearly identical for all schedulers. Despite the homogeneous nature of workload and machines, SOS maintains its scheduling principles and performs comparably to baseline schedulers.

These experiments show that *SOSA is an efficient, effective, and adaptable scheduler under varying realistic workloads targeting heterogeneous and homogeneous hardware.*

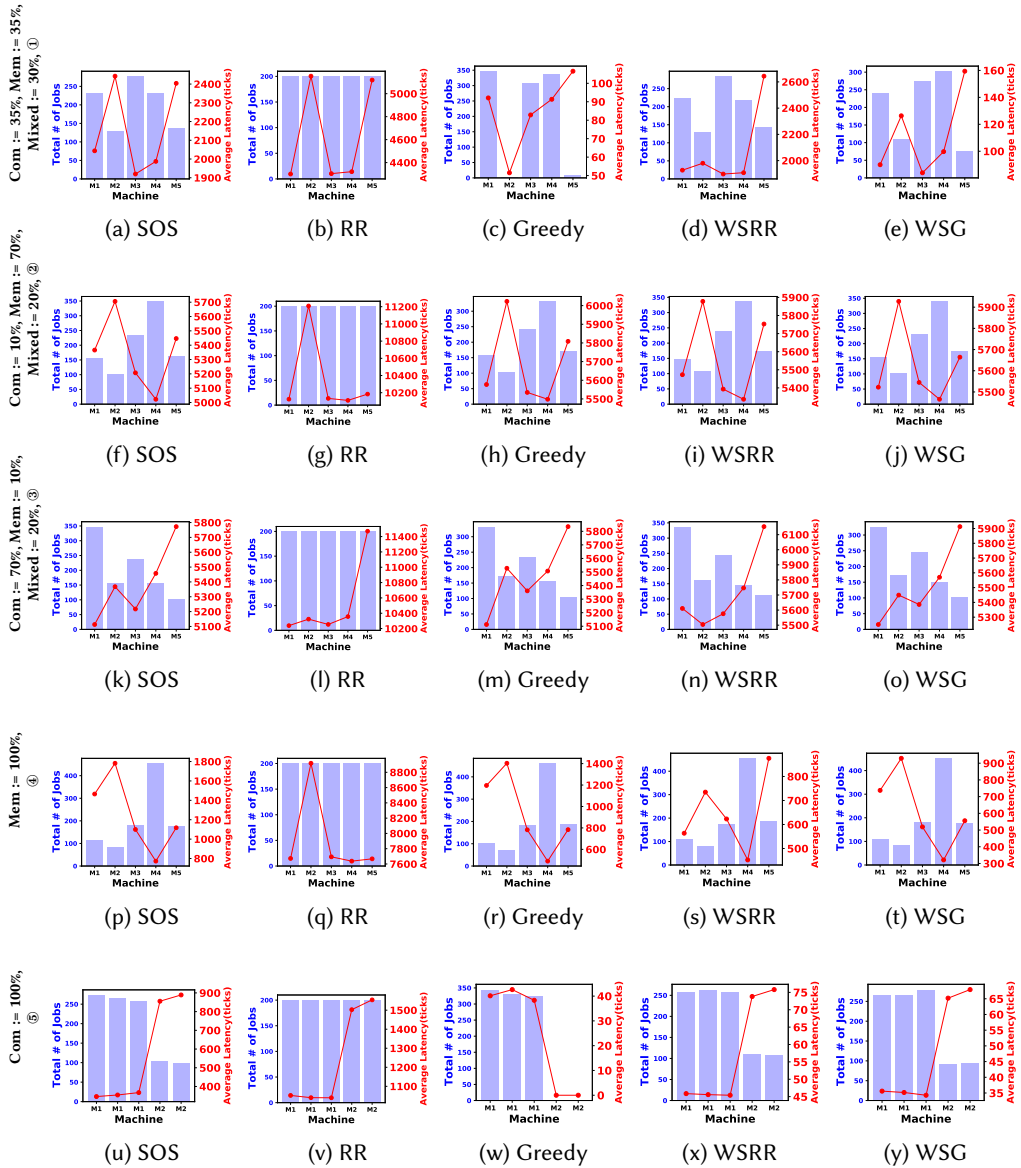


Fig. 18. Job distribution and average latency across M1 – M5 under varied workloads. SOS: Stochastic Online Scheduler; RR: Round Robin Scheduler; WSRR: Work Stealing Round Robin Scheduler; WSG: Work Stealing Greedy Scheduler.

9 Related Work

Several hardware-based schedulers have been developed for multicore systems. SR-PQ [15, 31] enabled configurable real-time scheduling with limited scalability. HRHS [5] improved flexibility

through partitioned scheduling, while TCOM [20] extended support for task dependencies. HD-CPS [29] addressed communication bottlenecks using per-core queues and priority drift using centralized coordination and SchedTask [14] reduced I-cache pollution by grouping tasks with similar instruction footprints but introduced hardware overhead and latency. Heuristics-based [9, 11, 34] and dynamic allocation methods [32] improve system utilization with increased scheduling overhead or inconsistent convergence. Learning-based schedulers [7] adapt to workloads while OPADCS [18] prioritizes deadline adherence in uncertain, online scenarios. Additional software-based efforts target optimal task mapping [21], system reliability [19], and energy-constrained execution [26]. **However, none of these approaches address heterogeneous stochastic online scheduling, and thus, direct comparison to SOSA is not applicable.**

Of pre-existing related works, the most relevant prior work can be found in Hardware HEFT [10]. In this work, the authors present a hardware-accelerated version of the Heterogeneous Earliest Finish Time scheduling algorithm. In their paper, they use their accelerator to perform scheduling decisions in a small SoC context consisting of up to 16 processing elements of two distinct types: either an ARM core or an FFT processing module. In this sense, SOSA (specifically in the STANNIC implementation) displays the capability of addressing significantly larger systems with higher levels of heterogeneity. Additionally, while HW-HEFT is demonstrated to be a capable SoC scheduler in dealing with dynamically arriving tasks by performing real-life signal processing, it also requires knowledge of all tasks, ahead of time, making it non-applicable to full stochastic online task arrival. This makes it a great fit for smaller, individual SoCs, but in larger, shared/networked systems, these unknowns may make HW-HEFT falter.

10 Conclusion

We introduced two hardware-accelerated online scheduler accelerator architectures, HERCULES and STANNIC, collectively referred to as SOSA. These architectures accelerate an algorithm capable of adapting to diverse workloads targeting heterogeneous and homogeneous computing systems with acceptable latency, and job distribution while minimizing expected job completion times. Both SOSA architectures consume only 21 Watts and achieve a speedup of 1968 \times compared to a C-based single thread scheduler. Such characteristics make SOSA a prime candidate for scheduling scientific and deep-learning workloads with significant variability.

The two architectures are presented chronologically in their development, allowing for iteration and optimizations to be explored in a solution-driven manner to justify the need for such a fundamental shift in architectural paradigm. Though the differences in operation are significant, parity in the two designs' function output was established, showing that the difference in function performance has no effect on the resultant schedules effectiveness. The finer details of scheduling with this new design, and proof of the required assumptions, were also provided.

With the two architectures now fully understood, we were able to measure performance metrics of both to quantitatively compare the two to each other. In every metric, STANNIC outperforms HERCULES, all while maintaining an equivalent power profile. STANNIC is on average 7.5 times faster than HERCULES, 2.1 \times smaller than HERCULES, and is capable of scaling to consider systems that are 14 times larger than HERCULES could consider, all while maintaining minimal power usage. Through these qualitative comparisons, we can see that STANNIC is a fundamentally more efficient and capable scheduling accelerator than HERCULES.

References

- [1] AMD. 2024. AMD Alveo U55C Product brief. <https://www.amd.com/en/products/accelerators/alveo/u55c.html>. Accessed: March 24, 2026.

- [2] AMD. 2024. AMD Vitis User Guide. https://docs.amd.com/r/en-US/Vitis_Libraries/User-Guide. Accessed: March 24, 2026.
- [3] Hongzheng Chen, Niansong Zhang, Shaojie Xiang, Zhichen Zeng, Mengjia Dai, and Zhiru Zhang. 2024. Allo: A Programming Model for Composable Accelerator Design. *ACM SIGPLAN Conf. on Programming Language Design and Implementation (PLDI)* (2024).
- [4] Yu-Hsin Chen, Tushar Krishnar, Joel S. Emer, and Vivienne Sze. 2017. Eyeriss: An Energy-Efficient Reconfigurable Accelerator for Deep Convolutional Neural Networks. *IEEE Journal of Solid-State Circuits* 52, 1 (2017), 127–138. doi:10.1109/JSSC.2016.2616357
- [5] Danesh Derafshi, Amin Norollah, Mohsen Khosroanjani, and Hakem Beitollahi. 2020. HRHS: A High-Performance Real-Time Hardware Scheduler. *IEEE Trans. on Parallel and Distributed Systems (TPDS)* (2020).
- [6] Ziqian Dong, Ning Liu, and Roberto Rojas-Cessa. 2015. Greedy Scheduling of Tasks With Time Constraints for Energy-Efficient Cloud-Computing Data Centers. *Journal of Cloud Computing* (2015).
- [7] Peilun Du, Zichang Sun, Haitao Zhang, and Huadong Ma. 2019. Feature-Aware Task Scheduling on CPU-FPGA Heterogeneous Platforms. *Int'l Conf. on High Performance Computing and Communications (HPCC)* (2019).
- [8] A. Epstein, G.U. Paul, B. Vettermann, C. Boulin, and F. Klefenz. 2002. A parallel systolic array ASIC for real-time execution of the Hough transform. *IEEE Transactions on Nuclear Science* 49, 2 (2002), 339–346. doi:10.1109/TNS.2002.1003733
- [9] Juan Fang, Jiaxing Zhang, Shuaibing Lu, and Hui Zhao. 2020. Exploration on Task Scheduling Strategy for CPU-GPU Heterogeneous Computing System. *IEEE Computer Society Annual Symp. on VLSI (ISVLSI)* (2020).
- [10] Alexander Fusco, Sahil Hassan, Joshua Mack, and Ali Akoglu. 2022. A Hardware-based HEFT Scheduler Implementation for Dynamic Workloads on Heterogeneous SoCs. In *2022 IFIP/IEEE 30th International Conference on Very Large Scale Integration (VLSI-SoC)*. 1–6. doi:10.1109/VLSI-SoC54400.2022.9939623
- [11] Mohammad Navid Habibpour Roudsari. 2024. Improved Task Scheduling in Heterogeneous Distributed Systems using Intelligent Greedy Harris Hawk Optimization Algorithm. *Evol. Intel. (EI)* (2024).
- [12] Tsung-Wei Huang, Dian-Lun Lin, Yibo Lin, and Chun-Xun Lin. 2022. Taskflow: A General-Purpose Parallel and Heterogeneous Task Programming System. *IEEE Trans. on Computer-Aided Design of Integrated Circuits and Systems (TCAD)* (2022).
- [13] Sven Jäger. 2023. An Improved Greedy Algorithm for Stochastic Online Scheduling on Unrelated Machines. *Discrete Optimization (DO)* (2023).
- [14] Prathmesh Kallurkar and Smruti R Sarangi. 2017. SchedTask: A Hardware-Assisted Task Scheduler. *Int'l Symp. on Microarchitecture (MICRO)* (2017).
- [15] Pramote Kuacharoen, Mohamed Shalan, and Vincent John Mooney. 2003. A Configurable Hardware Scheduler for Real-Time Systems. *Engineering of Reconfigurable Systems and Algorithms* (2003).
- [16] Yi-Hsiang Lai, Yuze Chi, Yuwei Hu, Jie Wang, Cody Hao Yu, Yuan Zhou, Jason Cong, and Zhiru Zhang. 2019. HeteroCL: A Multi-Paradigm Programming Infrastructure for Software-Defined Reconfigurable Computing. *Int'l Symp. on Field-Programmable Gate Arrays (FPGA)* (2019).
- [17] Yi-Hsiang Lai, Hongbo Rong, Size Zheng, Weihao Zhang, Xiuping Cui, Yunshan Jia, Jie Wang, Brendan Sullivan, Zhiru Zhang, Yun Liang, Youhui Zhang, Jason Cong, Nithin George, Jose Alvarez, Christopher Hughes, and Pradeep Dubey. 2020. SuSy: A Programming Model for Productive Construction of High-Performance Systolic Arrays on FPGAs. In *2020 IEEE/ACM International Conference On Computer Aided Design (ICCAD)*. 1–9.
- [18] Yifan Liu, Jinchao Chen, Jiangong Yang, Chenglie Du, and Xiaoyan Du. 2024. Uncertainty-Aware Online Deadline-Constrained Scheduling of Parallel Applications in Distributed Heterogeneous Systems. *Computers & Industrial Engineering* (2024).
- [19] Ajeya Naithani, Stijn Eyerman, and Lieven Eeckhout. 2017. Reliability-Aware Scheduling on Heterogeneous Multicore Processors. *Int'l Symp. on High-Performance Computer Architecture (HPCA)* (2017).
- [20] Amin Norollah, Zahra Kazemi, Niloufar Sayadi, Hakem Beitollahi, Mahdi Fazeli, and David Hely. 2021. Efficient Scheduling of Dependent Tasks in Many-Core Real-Time System Using a Hardware Scheduler. *Workshop on High-Performance Embedded Computing* (2021).
- [21] Michael Orr and Oliver Sinnen. 2021. Optimal Task Scheduling for Partially Heterogeneous Systems. *Parallel Comput.* (2021).
- [22] Vairavan* Palaniappan, Adam* Ross, Amit Ranjan Trivedi, and Debjit Pal. 2025. HERCULES: Hardware Accelerator for Stochastic Scheduling in Heterogeneous Systems. *Int'l Conf. on Computer-Aided Design (ICCAD)* (2025).
- [23] Juhua Pu, Qiaolan Meng, Yexuan Chen, and Hao Sheng. 2023. MPEFT: A novel task scheduling method for workflows. *Frontiers in Environmental Science* Volume 10 - 2022 (2023). doi:10.3389/fenvs.2022.996483
- [24] Patrice Quinton. 1987. An introduction to systolic architectures. In *Proc. of an Advanced Course on Future Parallel Computers*. (Pisa, Italy). Springer-Verlag, Berlin, Heidelberg, 387–400.

- [25] Naveen R and Sudhish N George. 2024. Power Efficient ASIC Design for Vision Transformer using Systolic Array Matrix Multiplier. In *2024 28th International Symposium on VLSI Design and Test (VDAT)*. 1–6. doi:10.1109/VDAT63601.2024.10705728
- [26] Valon Raca, Seeun William Umboh, Eduard Mehofer, and Bernhard Scholz. 2022. Runtime and Energy Constrained Work Scheduling for Heterogeneous Systems. *The Journal of Supercomputing (JSC)* (2022).
- [27] CPP Reference. 2024. popcount. <https://en.cppreference.com/w/cpp/numeric/popcount>. Accessed: March 24, 2026.
- [28] Kaz Sato and Cliff Young. 2017. An in-depth look at Google’s first tensor processing unit (TPU) | google cloud blog. <https://cloud.google.com/blog/products/ai-machine-learning/an-in-depth-look-at-googles-first-tensor-processing-unit-tpu>
- [29] Mohsin Shan and Omer Khan. 2022. HD-CPS: Hardware-Assisted Drift-Aware Concurrent Priority Scheduler for Shared Memory Multicores. *Int’l Symp. on High-Performance Computer Architecture (HPCA)* (2022).
- [30] Abraham Silberschatz, Peter B. Galvin, and Greg Gagne. 2012. *Operating System Concepts* (9 ed.). John Wiley & Sons.
- [31] Yi Tang and Neil W. Bergmann. 2015. A Hardware Scheduler Based on Task Queues for FPGA-Based Embedded Real-Time Systems. *IEEE Trans. on Computers (TC)* (2015).
- [32] Lanjun Wan, Weihua Zheng, and Xinpan Yuan. 2021. Efficient Inter-Device Task Scheduling Schemes for Multi-Device Co-Processing of Data-Parallel Kernels on Heterogeneous Systems. *IEEE Access* (2021).
- [33] Haroon Waris, Chenghua Wang, Weiqiang Liu, and Fabrizio Lombardi. 2021. AxSA: On the Design of High-Performance and Power-Efficient Approximate Systolic Arrays for Matrix Multiplication. *Journal of Signal Processing Systems* 93 (06 2021). doi:10.1007/s11265-020-01582-7
- [34] Serif Yesil and Ozcan Ozturk. 2022. Scheduling for Heterogeneous Systems in Accelerator-Rich Environments. *The Journal of Supercomputing (JSC)* (2022).
- [35] C. W. Yu, K. H. Kwong, K. H. Lee, and P. H. Leong. 2003. A Smith-Waterman systolic cell. *Lecture Notes in Computer Science* (Sep 2003), 375–384. doi:10.1007/978-3-540-45234-8_37

Received 20 February 2007; revised 12 March 2009; accepted 5 June 2009